Dosimetric considerations for patients with HIP prostheses undergoing pelvic irradiation. Report of the AAPM Radiation Therapy Committee Task Group 63

Chester Reft
University of Chicago, Chicago, Illinois 60637

Rodica Alecu
U.S. Oncology, Texas Cancer Center, Sherman, Texas

Indra J. Das
University of Pennsylvania, Philadelphia, Pennsylvania

Bruce J. Gerbi
University of Minnesota Medical School, Minneapolis, Minnesota

Paul Keall
Virginia Commonwealth University, Richmond, Virginia

Eugene Lief
New York University Medical Center, New York

Ben J. Mijnheer
Netherlands Cancer Institute, Amsterdam, Netherlands

Nikos Papanikolaou
University of Arkansas Medical Sciences

Claudio Sibata
East Carolina University School of Medicine, Greenville, North Carolina

Jake Van Dyk
London Regional Cancer Centre, Ontario, Canada

(Received 25 July 2002; accepted for publication 10 February 2003; published 30 May 2003)

This document is the report of a task group of the Radiation Therapy Committee of the AAPM and has been prepared primarily to advise hospital physicists involved in external beam treatment of patients with pelvic malignancies who have high atomic number (Z) hip prostheses. The purpose of the report is to make the radiation oncology community aware of the problems arising from the presence of these devices in the radiation beam, to quantify the dose perturbations they cause, and, finally, to provide recommendations for treatment planning and delivery. Some of the data and recommendations are also applicable to patients having implanted high-Z prosthetic devices such as pins, humeral head replacements. The scientific understanding and methodology of clinical dosimetry for these situations is still incomplete. This report is intended to reflect the current state of scientific understanding and technical methodology in clinical dosimetry for radiation oncology patients with high-Z hip prostheses. [DOI: 10.1118/1.1565113]

Key words: hip prosthesis, dose perturbation

TABLE OF CONTENTS

I. INTRODUCTION

The success or failure of radiation therapy treatments depends upon the accuracy with which the dose prescription is fulfilled. For many diseases, the outcome of the treatment depends upon the dose being delivered to an accuracy of $\pm 3\%-4\%$ (one standard deviation).[1,2] This is a stringent requirement for routine treatments and is difficult to achieve if all sources of treatment uncertainty are evaluated. Most of the national and international guidelines[3–7] for consistency and accuracy in radiation dosimetry provide information for homogeneous media, but the human body consists of many components that deviate significantly from unit density, e.g., bone, lung, teeth, air cavities, and small intercalated spaces within bone. In addition to these naturally occurring internal inhomogeneities, man-made materials may also be present such as mandibular plates for reconstruction, hip, leg, and arm prostheses, spinal cord fixation devices, surgical rods, stents, and various dental fillings. In this report we focus on hip prostheses. These devices are usually made from high atomic number (high-Z) elements. In this study high-Z is defined as a material with atomic number greater than cortical bone. In megavoltage photon beams these materials have the potential to greatly affect the dose delivered to the prescription point and to tissue shielded by the prosthesis. Consequently, dramatic differences in the treatment outcome from what was originally intended can result.

As the population ages and the use of hip prostheses become more common, the problem of treating these patients will also increase. Although at this time there are few data showing a decrease in tumor control due to the reduced target dose from shadowing of the prosthesis, or an increase in the complication rates due to the dose perturbation by the presence of metallic implants, problems could arise in the future. In groin irradiation for gynecological malignancies using opposed anterior/posterior fields, Grigsby *et al.*[8] reported hip fractures in patients at doses greater than 50 Gy. But, to the best knowledge of this group, no quantitative data are available on the effects of the increased dose at the interface between a hip prosthesis and surrounding tissue in patients undergoing radical treatment of tumors in the pelvic region. However, if dose escalation continues in treating pelvic tumors, the decreased tumor dose and the increased dose near the bone-metal interface could become factors in tumor control and radiation complications such as bone necrosis and weakening of the fixation of the implant.

A survey of 30 institutions conducted by this task group showed that the number of patients with prosthetic devices, which could affect their radiation therapy, was 1%–4% of the total number of patients. No general consensus on how to manage the treatment of these cases was observed. Some institutions ignore the presence of the device altogether. Other institutions modify the beam orientation to avoid the device even if the result is to give additional dose to critical structures adjacent to the planning target volume. Sometimes treating through sensitive structures is an appropriate solution to the problem if the total prescribed dose is low enough so that the resultant dose to the structure is below the tolerance dose. Some institutions try to account for the presence of the device by using computer treatment planning programs or hand calculations involving a correction for the attenuation of the device. Others may fabricate compensators to correct the dose distribution in the target while some may use a combination of these approaches. The increasing availability of intensity modulated radiation therapy may offer a method for treating these patients. All the survey respondents acknowledged that high-Z devices constitute a problem with the patient's treatment and that recommendations for dealing with these situations would be useful. In response to these concerns, this task group was formed to identify the problems caused by the presence of high-Z hip prostheses in pelvic megavoltage photon radiation treatments. Practical suggestions are given for dealing with the presence of prostheses and to minimize, or at least quantify, their undesired effects, while reducing the impact to the surrounding critical structures.

II. RADIATION PHYSICS CONSIDERATIONS

The presence of a high-Z inhomogeneity in an irradiated water phantom or patient results in attenuation of the radiation through the inhomogeneity as well as local perturbations known as interface effects. There are numerous reports[9–30] on attenuation effects in non-tissue-equivalent materials. Figure 1 illustrates the perturbations to the central axis depth dose curve for 6 and 18 MV broad radiation beams incident on a water phantom containing an infinitely wide 3 cm Co–Cr–Mo slab from depths 5 to 8 cm. Three dose regions are shown in the figure. Region 1 is a distance greater than $d_{\max}$ from the implant, and regions 2 and 3 are at the proximal and distal ends of the implant, respectively. The central axis depth doses in region 1 shown in Figs. 1(a) and 1(b) are at a distance greater than $d_{\max}$ from the inhomogeneity, and illustrate the effects of absorption and scatter by the implant. The beam attenuation in the material is somewhat offset by the in-scatter from the unobstructed portion of the beam. For a smaller beam that just encompasses the implant, the curve would run parallel to the unattenuated curve since there would be a smaller contribution from in-scatter by the unobstructed portion of the beam. However, since treatment fields for the pelvis are generally larger than the inhomogeneity, in-scatter from the unobstructed portion of the beam partially compensates for the loss of dose due to attenuation distal to the inhomogeneity. The magnitude and the spatial extent of these effects depend on the energy of the radiation as well as the density, atomic number, and dimensions of the inhomogeneity. For photon beams above 10 MV, there are gamma-rays produced by interactions of contaminant neutrons with the high-Z material. These are not included in the Monte Carlo simulation, but will be shown (Sec. IV B 3) to contribute little dose to tissue around a prosthesis.

The decrease in intensity of the radiation at distances greater than the secondary electron range downstream from the inhomogeneity can be calculated with knowledge of the density and atomic number of the material and its linear or mass attenuation coefficients (μ and μ/ρ, respectively). The

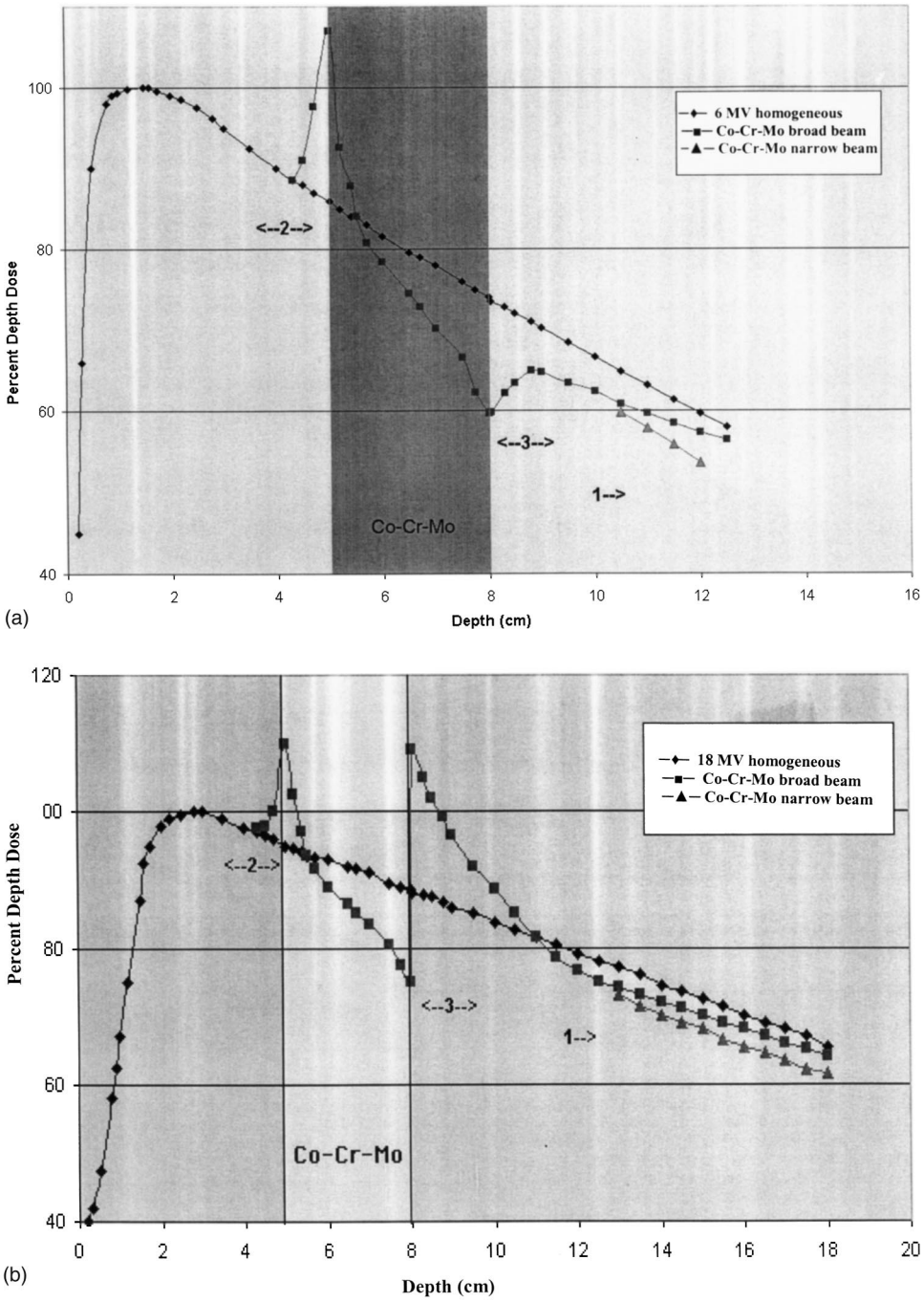

FIG. 1. Dose perturbation near and far from a Co–Cr–Mo inhomogeneity. (a) and (b) show the perturbation to the central axis percentage depth dose for 6 and 18 M beams incident on a 3 cm thick Co–Cr–Mo slab inhomogeneity. Region 1 is greater than d_{max} from the implant and zones 2 and 3 are at the proximal and distal ends of the implant, respectively.

primary fluence beyond the metallic implant is approximately given by

$$\psi = \psi_0 e^{-\mu t}, \tag{1}$$

where ψ is the photon fluence after passing through a thickness t of high-Z material, ψ_0 is the initial fluence, and μ is the total composite linear attenuation coefficient including the various interactions: photoelectric (τ), Compton (σ), and pair production (κ) averaged over the photon spectrum:

$$\mu = \tau + \sigma + \kappa. \tag{2}$$

It is more difficult to account for the contribution of scattered photons and the effects of electron disequilibrium. Approximate methods (e.g., effective TMR ratios to partially account for scatter) are described in Sec. IV B 1. The problems associated with the interface effect are much more complex, but probably less clinically important within the context of hip prosthesis. Various researchers in their publications describe quantitatively the dose perturbation that occurs at the high-Z interface.[13,31–56] At the interface between bone and prosthesis, the dose perturbation is similar to that at a tissue/high-Z interface, albeit the magnitude and extent of the effects will be diminished due to a closer match between the atomic numbers of the two materials. Perturbations in the dose distributions in regions 2 and 3 (Fig. 1) occur near the interface

TABLE I. BSDF versus distance from interface for $10\times10\ \text{cm}^2$ where BSDF$=D_i/D_h$ and D_i and D_h are the doses with and without the presence of the interface, respectively.

Material	Bone		Lead	
Density (g/cm^3)	1.83		11.4	
Atomic no.	13		82	
Distance (cm)	6 MV	18 MV	6 MV	18 MV
0.1	1.03	1.04	1.34	1.45
0.2	1.01	1.02	1.20	1.30
0.4	1.01	1.01	1.01	1.14
1.0	1.00	1.00	1.00	1.06
1.4	1.00	1.00	1.00	1.03

TABLE II. FDPF versus distance from the interface for $10\times10\ \text{cm}^2$ where FDPF$=D_i/D_h$ and D_i and D_h are the doses with and without the presence of the interface, respectively.

Material	Bone		Steel		Lead	
Density (g/cm^3)	1.83		7.76		11.4	
Thickness (g/cm^3)	1.83		2.56		2.28	
Atomic no.	13		26		82	
Distance (cm)	6 MV	18 MV	6 MV	18 MV	6 MV	18 MV
0.05	0.94	1.05	0.85	1.20	0.84	1.41
0.1	0.95	0.04	0.87	1.19	0.85	1.40
0.5	0.98	1.03	0.92	1.15	0.88	1.29
1.0	0.99	1.02	0.94	1.11	0.91	1.21
2.0	0.99	1.01	0.95	1.05	0.93	1.10
4.0	0.99	1.00	0.94	0.98	0.93	0.98
6.0	0.99	0.99	0.94	0.96	0.93	0.94

and extend a distance approximately $d_{\max}$ from it. On both sides of a high-Z material within the homogeneous medium, there are rapid changes in dose due to electron transport, which extends into each medium over a distance of the order of the range of the secondary electrons. These effects are illustrated in Figs. 1(a) and 1(b) for 6 and 18 MV beams, respectively. This dose may be higher or lower than that at the same geometric depth in a homogeneous medium. The dose perturbation depends upon the incident photon energy, differences in the photon energy transfer coefficients, the atomic number (Z), the mass density and thickness of the inhomogeneity, and the differences in multiple scatter of the secondary electrons. For energies greater than 10 MV there may be an increased dose distal to the high-Z material that is attributed to pair-production interactions in the metal. Lateral to the inhomogeneity, the electron fluence increases due to the increased lateral scattering from the material producing an increased dose to the surrounding tissue. A dose correction factor (CF) can be defined as the ratio of doses with (D_i) and without (D_h) the presence of the interface as

$$\mathrm{CF}(E,A,A_p,d,t,x,\mathrm{Z},\rho,\theta)=D_i/D_h, \tag{3}$$

where E is the beam energy, A is the field size, A_p is the area of the prosthesis from the beam's perspective, d is the depth of the interface from the surface, t is the thickness of the high-Z medium creating the interface with the soft tissue (low-Z), x is the distance either proximal or distal from the interface to the point where the dose is estimated, Z and ρ are the atomic number and physical density of the inhomogeneity, respectively, θ is the beam angle relative to the implant, D_i is the dose in the presence of the interface, and D_h is the dose in a homogeneous medium. Although there are very limited data on the interface effect and beam angle, Nadrowitz and Feyerabend[57] reported it to be an important parameter. However, for a cylindrical prosthetic geometry, θ can be ignored in the equation. Furthermore, the CF can be separated into two components: the backscattered dose perturbation factor (BSDF[31]) at the entrance side of the high-Z inhomogeneity, and the forward dose perturbation factor (FDPF[43,44]) on the exit side of the inhomogeneity. The magnitude and the extent of the above effects are shown in Tables I and II for a slab inhomogeneity (bone, steel and lead) for 6 and 18 MV photon beams[58] in a water-equivalent phantom. Except in the build-up region, the correction factors are independent of the depth of the high-Z material. For the given material thickness the FDPF behaves significantly different with energy than the BSDF. At the interface for 6 MV it varies from 0.94 to 0.84 for bone and lead, and for 18 MV, it varies from 1.05 to 1.41 for bone and lead, respectively. The magnitude of BSDF is between 1.08 and 1.70 for bone and lead, respectively, and falls off rapidly from the interface. Although we are unaware of published data for correction factors at a bone/high-Z interface, we expect the effect to be smaller than that at a tissue/high-Z interface by approximately the ratio of their atomic numbers. Ding and Yu[9] using Monte Carlo simulations investigated the interface effects for parallel-opposed photon beams.

Gullane[56] measured doses at interfaces using a wall-less ionization chamber. Figures 2(a)–2(d) show results for stainless steel and titanium for both single and parallel-opposed beams. The interface doses increase by as much as 50% at the proximal surface of the metallic inhomogeneity.

Erlanson *et al.*,[18] using small Si diodes, measured the dose increase at the distal site behind a titanium alloy prosthesis in a water phantom for photon energies of 6, 20, and 50 MV. They concluded that for radiation therapy in the pelvic region using a four-field box technique, the mean dose close to the prosthesis is below the prescription dose of 65 Gy and below the critical level of complications, i.e., even a 25% increase in dose over that for a normal hip in a small volume near the prosthesis is not expected to result in an increase in morbidity. However, escalation of the prescription dose and the enhanced dose at the bone–prosthesis interface could increase the probability for bone necrosis. The normal tissue complication probability doses for bone necrosis are estimated to be 52 and 65 Gy for the complication probabilities of 5% in 5 years (TD 5/5) and 50% in 5 years (TD 50/5), respectively.[59,60] There are on-going dose escalation studies for treating the prostate. The Radiation Therapy Oncology Group (RTOG) closed a protocol (94-06) in which the prescribed dose was 78 Gy. Some institutions treat high-risk prostate patients to 86.4 Gy by using field arrangements that avoid the prosthesis. Depending upon the field arrange-

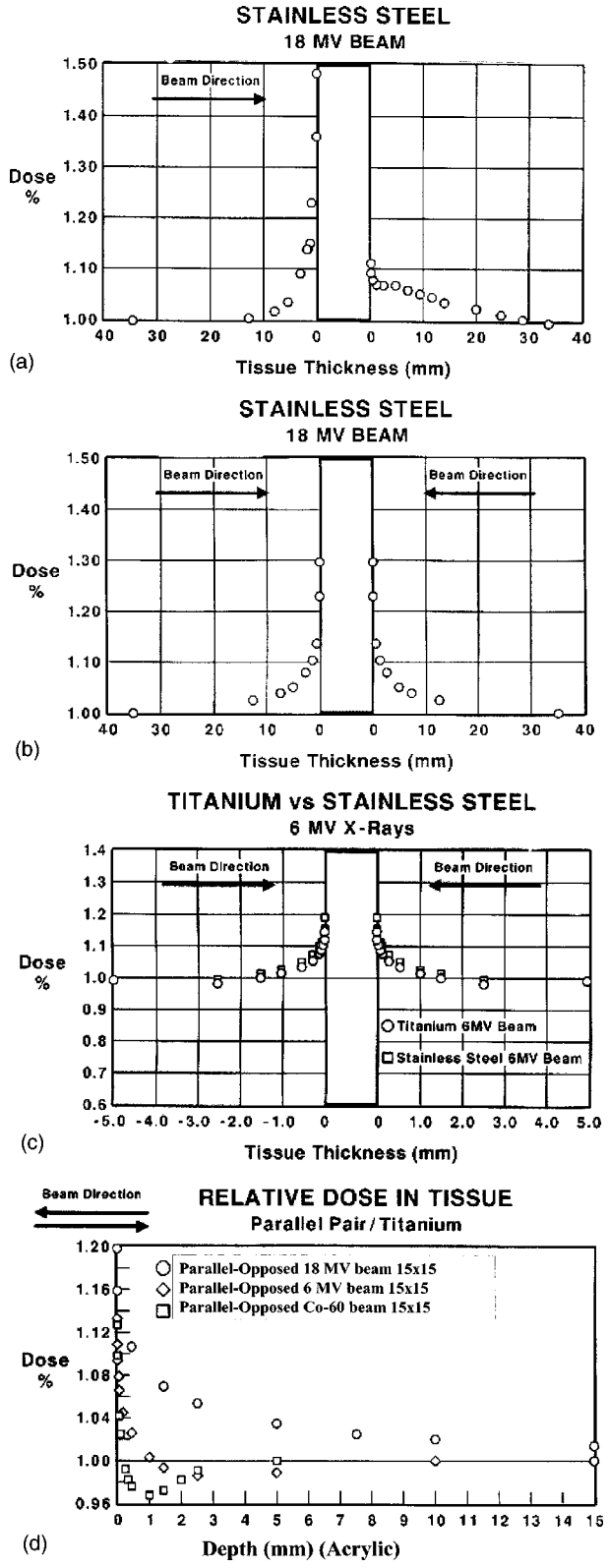

FIG. 2. High Z-tissue-metal interface effects for 15×15 cm^2 field. The data are normalized to 1.00 at a distance from the interface greater than the range of the electrons set in motion. (a) Dose perturbations due to a stainless steel plate for a single 18 MV unidirectional beam. (b) Dose perturbations due to a stainless steel plate for parallel-opposed 18 MV beams. (c) Relative dose in tissue on both sides of a Ti or steel plate irradiated by parallel-opposed 6 MV beams. (d) Relative dose in acrylic on one side of Ti irradiated by parallel-opposed ^{60}Co, 6 MV and 18 MV beams (Ref. 56).

ments and the beam energy, there is the potential for an enhanced dose near the prosthesis–bone interface that could potentially increase the incidence of bone necrosis. Most current treatment planning systems account for beam attenuation, if the composition of the inhomogeneity is known, and the CT number to electron density conversion curve is suitable. However, only Monte Carlo based treatment planning systems promise the ability to calculate the dose accurately near a high-Z inhomogeneity.

III. HIP PROSTHESES—GENERAL PROPERTIES

There are many designs of hip prostheses [see Fig. 3(a)]. Usually, a total hip replacement will include a prosthetic acetabular cup and a femoral component. The acetabular cup consists of a polyethylene core supported by either a Co–Cr–Mo or Ti alloy outer shell. The femoral component consists of a stem and a head, which can be hollow or solid, made of Co–Cr–Mo, Ti alloy, or steel. Some patients might have all three components, while others might have only the femoral stem implanted. The physical properties that are important dosimetrically are hollowness, shape, size, and composition. The majority of the current hip prosthetic devices are made of Co–Cr–Mo alloys. Stainless steel was used in the past, and may still be found in patients with older implants. Titanium is also used in some cases.

A thorough study on the influence of hip prostheses on the dose distribution was reported by Sibata *et al.*[12] for incident 6 and 18 MV photon fields. In this study, prosthetic devices from several manufacturers were used. Table III(a), from Sibata *et al.*,[12] gives the common composition of the alloys used in the manufacture of the hip prosthesis devices and the calculated electron densities of the alloys relative to water. The physical properties, such as mass density, mass attenuation coefficient, effective atomic number, electron density, and relative electron density for the three most common types of hip prosthesis are provided in Table III(b) from Hazuka *et al.*[14] A difference as high as 17%–19% is shown between the physical density and the relative electron density of each alloy, the difference being much larger than the one calculated for biologically equivalent materials.[14] The relative electron densities of similar types of prosthetic devices are slightly different in the two sets of data presented in Tables III(a) and (b).

Besides the use of metals for prosthetic materials, ceramic and synthetic materials are occasionally used as implants for surgery. Ball heads of densely sintered, high-purity alumina (Al_2O_3) ceramic and polyethylene have been used for prosthetic parts. The mass density and relative electron density with respect to water for alumina are 3.97 g/cm^3 and 3.52, respectively. The dosimetric problems with these prostheses are expected to be smaller than those reported here on metallic prostheses because its electron density and effective atomic number ($\sim$16) are lower.

The effect of the radiation on the prosthetic materials is not of concern because published data[61] indicate that doses of the order of MGy are required to affect the mechanical properties of these materials.

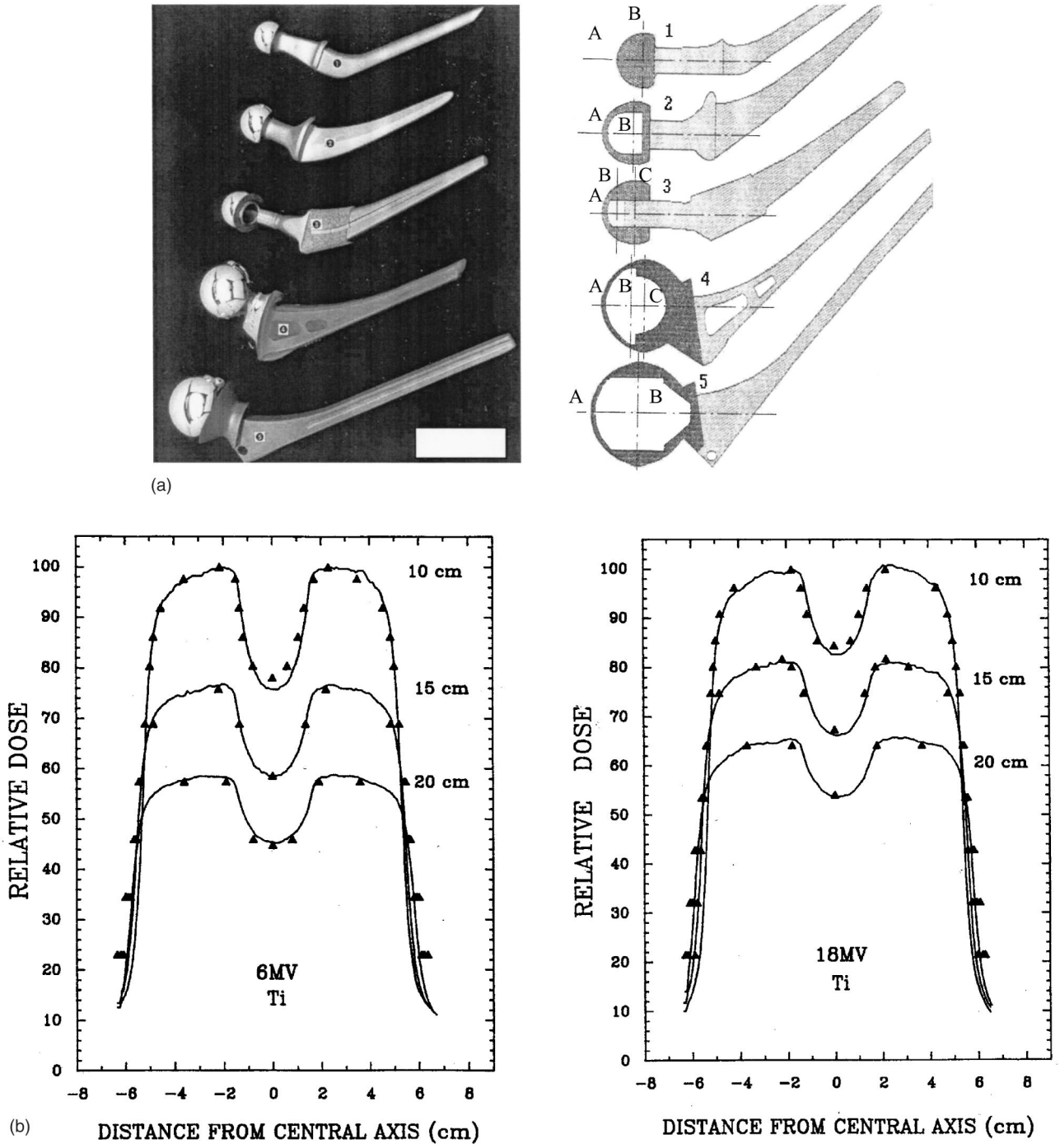

FIG. 3. (a) Prosthesis models and cross sections of the models. (b) Measured (−) versus calculated (▲) dose behind a titanium prosthesis at depths of 10, 15, and 20 cm for 6 and 18 MV beams (Ref. 12). Field size 10×15 cm^2, 100 cm SSD and the prosthesis is at a depth of 6.5 cm (reprinted from Ref. 12).

IV. QUANTIFICATION OF THE PERTURBATIONS PRODUCED BY PROSTHETIC DEVICES IN THE ABSORBED DOSE DISTRIBUTION

As previously mentioned, when a radiation beam passes through a prosthesis, perturbations of the absorbed dose distribution occur due to the increased attenuation of the beam by the prosthesis and interactions at the bone–metal interface. Several groups[11,12,14–17] have attempted to quantify these perturbations by measuring the dose—either in phantoms containing a prosthesis or in patients—or by calculating with a treatment planning system (TPS). Most prosthetic devices are made of Co–Cr–Mo or titanium alloy, so some of the measurement data in this report may also be useful for implants other than hip prostheses. However, one should be cautious in using these data for other type of implants because the size, shape, and composition of the device will

TABLE III. (a) Elemental composition of various prosthetic devices (Ref. 12). (b) Physical properties of some selected hip prostheses (Hazuka *et al.*, Ref. 14).

(a)

	Stainless steel wrought	Co-Cr-Mo cast-wrought	Titanium cast-wrought
(A) Composition of prosthesis alloys (%Weight)			
Element			
Carbon	0.08 max	0.35 max	0.08 max
Manganese	2.00 max	1.00 max	···
Phosphorus	0.03 max	···	···
Sulfur	0.03 max	···	···
Silicon	0.75 max	1.00 max	···
Oxygen	···	···	0.13 max
Cobalt	···	Balance (57.4–65)	···
Chromium	17–20	27–30	···
Nickel	10–14	2.50 max	···
Molybdenum	2–4	5–7	···
Iron	Balance (59–70)	0.75 max	0.25 max
Aluminum	···	···	5.6–6.5
Vanadium	···	···	3.5–4.5
Titanium	···	···	Balance (88.5–91)
(B) Electron density relative to water			
Range	6.55–6.61	6.79–6.90	3.72–3.76
Average	6.58	6.84	3.74

(b)

Prosthesis	Cross Sectional dimension (mm) Thickness× width	Physical density (g/cm^3)	Mass attenuation coefficient at 4 MV (cm^2/g)	Effective atomic no.	Electron density (e^-/cm^3)	Relative electron density
Stainless steel	11.4×20.0	8.1	0.047	26.7	2.3×10^{24}	6.83
Co–Cr–Mo	16.2 diameter	7.9	0.044	27.6	2.2×10^{24}	6.74
Titanium	13.6×15.0	4.3	0.048	21.4	1.2×10^{24}	3.6

strongly affect the dose perturbation. The measured magnitude of these effects is presented in this section for the three most common type hip prosthesis: Co–Cr–Mo, Ti, and steel.

A. Beam attenuation—measurements

Hazuka *et al.*[14] published data on the transmission factor through hip prosthesis devices made of Co–Cr–Mo, Ti, and steel for 4 and 10 MV photon beams. The transmission was measured in a water phantom with 0.1 cm^3 sealed ion chambers and with the beam positioned with its central axis passing through the approximate center of the solid stem of each prosthesis. Measured beam profiles were used to correlate beam transmission with the cross-sectional dimensions of each prosthesis. In each case, the prosthesis was positioned at 5 cm depth in water and measurements were made at 10 and 15 cm depth for 8×8 and 15×15 cm^2 field sizes. Their measurements are summarized in Table IV. The lowest transmission was measured for a Co–Cr–Mo prosthesis (0.657 for 4 MV photons). The transmission increased with field size and energy. The data show that for each prosthesis, at a given energy and depth, the transmission increases with the field size, due to the increased phantom scatter which partially offsets the shielding effect of the prosthesis. The increase in transmission ranged from 2% to 8% for the three prostheses used in these measurements, when the field size was increased from 8×8 cm^2 to 15×15 cm^2. The cross-sectional dimensions of the three prostheses are different; therefore, the differences in the transmission data cannot be attributed only to the material of the prosthesis. Data for prostheses fabricated from different materials with identical geometrical dimensions (28 mm prosthesis head diameter) were published by Sibata *et al.*,[12] for 6 and 18 MV photon beams. The cross sections of the prosthetic devices used in

TABLE IV. Transmission factors for 4 and 10 MV photon beams (Ref. 14) for the selected prostheses given in Table III(a).

Photon energy (MV)	4				10			
Field size (cm^2)	8×8		15×15		8×8		15×15	
Prosthesis/depth (cm)	10	15	10	15	10	15	10	15
Stainless steel	0.763	0.764	0.786	0.795	0.807	0.799	0.816	0.819
Co–Cr–Mo	0.657	0.672	0.708	0.714	0.735	0.736	0.748	0.749
Ti	0.861	0.855	0.869	0.876	0.887	0.879	0.891	0.894

TABLE V. Attenuation factors for 6 and 18 MV photon beams (Ref. 12), 15×15 cm^2 field size, at a depth of 10 cm for a selection of prostheses. The prostheses were set at 5 cm depth. Index of perturbation (IP) is the average attenuation for a given section (Fig. 3) of the prostheses.

			Maximum attenuation		IP	
Prosthesis	Alloy	Section	6 MV	18 MV	6 MV	18 MV
1	Co–Cr	A	0.45	0.35	0.29	0.22
		B	0.45	0.35	0.29	0.28
1	Ti	A	0.26	0.17	0.16	0.11
		B	0.26	0.17	0.21	0.15
2	Co–Cr	A	0.44	0.32	0.28	0.18
		B	0.36	0.25	0.27	0.20
2	Ti	A	0.28	0.20	0.18	0.14
		B	0.28	0.20	0.24	0.17
3	Co–Cr	A	0.42	0.30	0.21	0.14
		B	0.4	0.30	0.32	0.26
		C	0.42	0.31	0.36	0.28
4	S. steel	A	0.44	0.41	0.27	0.15
		B	0.24	0.14	0.08	0.05
		C	0.46	0.38	0.34	0.29
5	Co–Cr	A	0.50	0.37	0.20	0.15
		B	0.42	0.28	0.32	0.24

this study and their geometric properties are shown in Fig. 3(a). The effect of the prosthesis on the dose profiles at depths of 10, 15, and 20 cm for 6 and 18 MV beams for a titanium prosthetic device is presented in Fig. 3(b). The increased contribution from the phantom scatter with depth partially offsets the shielding effect of the prosthesis. The transmission also increases from hardening of the beam as it penetrates the device. The authors have further defined an index of perturbation (IP) to take into account the average attenuation over the geometry of the prosthetic device (Table V). This index is the average measured attenuation of the device in the plane of the cross section. The results show that the Co–Cr–Mo prosthesis produces the most attenuation.

For a Ti alloy prosthesis Eng[29] reported attenuation factors ranging from 0.64 to 0.39 and 0.60 to 0.32 for 6 and 15 MV photon beams, respectively. The magnitudes of these factors depend upon the thickness of the prosthesis at the point of measurement. Erlanson *et al.*,[18] using small Si diodes, measured the attenuation behind a titanium alloy prosthesis at different angles (20° and 90°) in a water phantom for photon energies of 6, 20, and 50 MV. Dose profiles at various depths and depth dose curves were measured with and without the prosthesis in place, at 5 cm depth, 100 cm target to surface distance. The effect of attenuation for a four-field technique was a decrease in the target dose ranging from 9.8% to 8.1% between 6 and 50 MV beams for equally weighted beams, and 6.2% to 5.2% for lightly weighted (50% weighted) lateral beams. This suggests that for a four-field technique the dose distribution is nearly independent of energy at the center of the target. However, close to the prosthesis the attenuation was dependent on the beam energy and the position of the prosthesis. For 50 MV a dose enhancement of about 25% was observed at the interface that extended up to 2 cm from the interface.

TABLE VI. Summary of mass attenuation coefficients μ/ρ (cm^2/g) (Ref. 62).

Energy (MeV)	Titanium (Z=22)	Iron (Z=26)	Cobalt (Z=27)
0.05	1.213	1.958	2.144
0.06	0.7661	1.205	1.314
0.08	0.4052	0.5952	0.6414
0.10	0.2721	0.3717	0.3949
0.15	0.1649	0.1964	0.2023
0.20	0.1314	0.1460	0.1476
0.30	0.1043	0.1099	0.1094
0.40	0.090 81	0.094 00	0.093 11
0.50	0.081 91	0.084 14	0.083 15
0.60	0.075 29	0.077 04	0.076 04
0.80	0.065 72	0.066 99	0.066 04
1.00	0.058 91	0.059 95	0.059 06
1.25	0.052 63	0.053 50	0.052 70
1.50	0.048 01	0.048 83	0.048 10
2.00	0.041 80	0.042 65	0.042 04
3.00	0.035 12	0.036 21	0.035 80
4.00	0.031 73	0.033 12	0.032 83
5.00	0.029 82	0.031 46	0.031 27
6.00	0.028 68	0.030 57	0.030 45
8.00	0.027 59	0.029 91	0.029 91
10.0	0.027 27	0.029 94	0.030 02
15.0	0.027 62	0.030 92	0.031 15
20.0	0.028 44	0.032 24	0.032 56

B. Treatment planning and manual dose calculation aspects

The calculation of the dose perturbations due to the beam attenuation, interface effects, and neutron production will be discussed in this section for the common types of hip prostheses. The published data[12,14,16,18] demonstrate that the changes in the dose distribution in the target volume depend upon the location of the prosthesis with respect to the planning target volume (PTV), the size, shape, and material of the prosthesis, as well as on the beam energy.

1. Beam attenuation

If the composition and type of the prosthesis is known, the dose attenuation can be estimated by accounting for attenuation and scatter of the beam using information from simulator films and portal images. A more accurate method is to use calculations obtained from treatment planning system software supported by CT data. If CT information is used, allowances for image artifacts created by the metallic device must be made as discussed in Sec. IV B 1 *d*. Since kilovoltage images provide no information on whether the prosthesis is solid or hollow, a portal image should be taken. From this information the beam attenuation can be calculated from tabulated mass attenuation coefficients (Table VI) (62) for the average photon energy. Alternatively, flat sheets of the appropriate material can be used to measure the effective attenuation coefficient in a tissue-equivalent phantom under broad beam geometry that approximates the clinical condition. These techniques will overestimate the attenuation because they do not account for the photon scatter. Alterna-

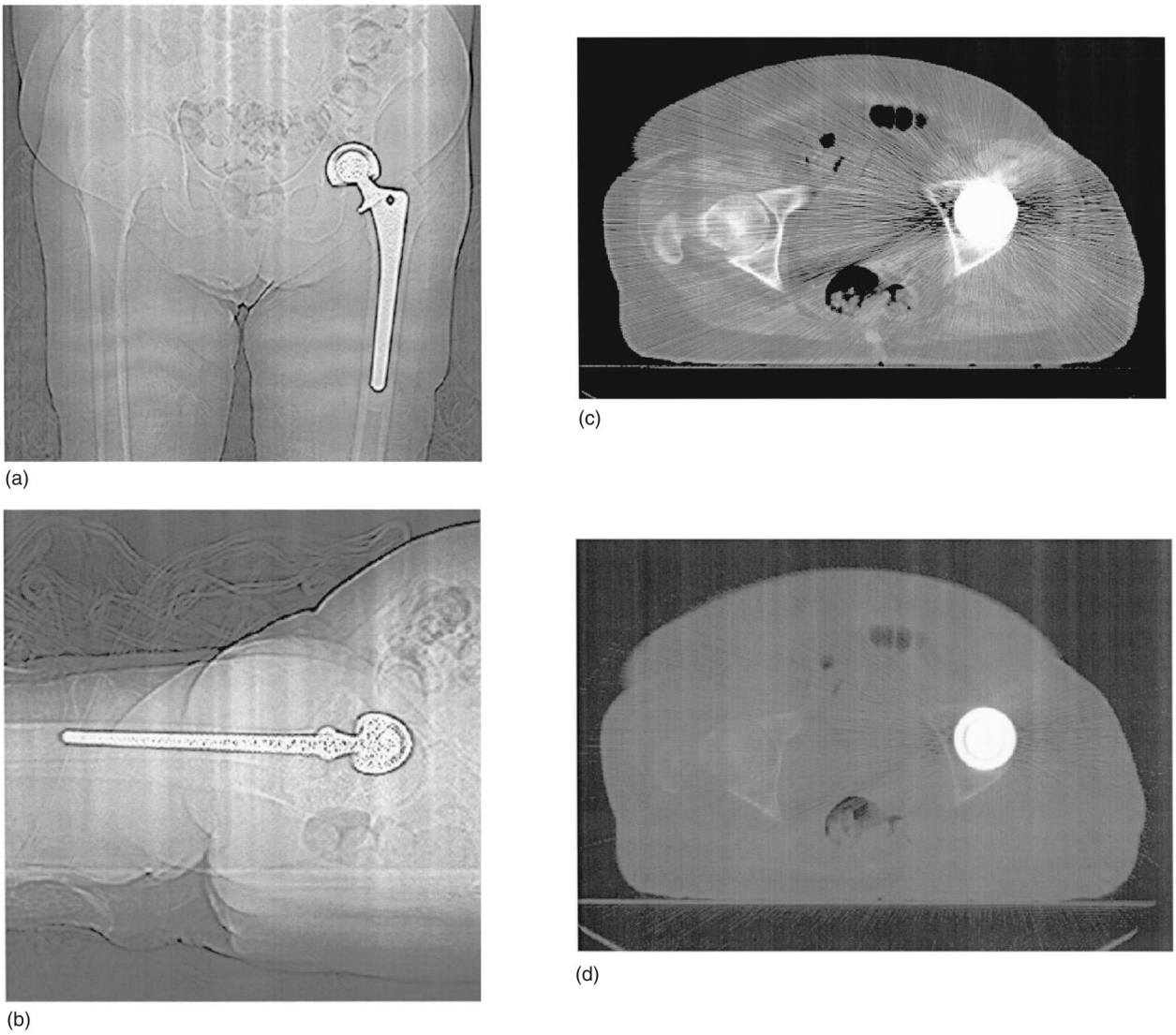

FIG. 4. CT images of a patient with a hip prosthesis (cup, head, and stem): (a) frontal image/scout, (b) lateral view scout, (c) transversal slice showing artifacts, and (d) same image as in (c), but contrast level adjusted to better visualize the contour of the prosthesis.

tively, exit dose measurements using detectors as discussed in Sec. IV C can be used to determine effective attenuation coefficients.

a. Manual calculations. If the dose calculation point is in a region where the assumption of charged particle equilibrium is a good approximation, that is, at a distance greater than $d_{\max}$ from the implant, manual calculations are the simplest way to estimate the attenuation of the prosthesis. The target dose can be quickly estimated using either of the two equations below: Eq. (4), which accounts for primary attenuation only, or Eq. (5), which accounts for attenuation and partially accounts for scatter. If the elemental composition of the prosthesis can be obtained from the manufacturer, one can calculate the approximate narrow beam attenuation coefficient as a weighted average, based on published tables.[62] However, estimates of 5% accuracy can be made by using the coefficients for iron, cobalt, or titanium for the three most frequently used prostheses (Table VI). From the dimensions of the prosthesis the transmission through the prosthesis can be determined using

$$I/I_0 = e^{-\mu t}, \tag{4}$$

where I/I_0 is the relative transmitted intensity and μ is a measured or calculated attenuation coefficient. The thickness, t, of the prosthesis at various levels of the CT slices, can be obtained from simulation films or CT scans [Figs. 4(a)–4(d)]. The attenuation calculated in this way overestimates the beam attenuation due to the prosthesis, because the narrow beam approximation does not take into account the "in-scattered" radiation, from the prosthesis or the patient. Scattering partially compensates for primary photon attenuation downstream from the prosthesis.

Scattering can be partially accounted for by using the effective tissue-air-ratio (TAR) or the tissue-maximum-ratio (TMR) methods.[63] The dose at a point behind the prosthesis,

D_i, can be calculated by applying a correction factor, CF, to the dose, D_h, at the same point in the absence of the prosthesis.

$$\mathrm{CF} = D_i(d',t)/D_h(d,t) = \mathrm{TMR}(d',w)/\mathrm{TMR}(d,w), \quad (5)$$

$$d' = d - t(1-\rho_e). \quad (6)$$

Here d' is the water-equivalent depth, t is the dimension of the prosthesis measured parallel to the axis of the beam, d is the calculation depth, ρ_e is the electron density of the prosthesis relative to water (Table III), and w is the effective field size. Ding and Yu[9] showed that this method can adequately predict the dose correction factor for the prosthesis when its mass density is used to calculate the water-equivalent depth. It was an empirical finding from their work that there was better agreement between measurement and calculation using the mass density rather than the electron density. As an example, for a 1.6 cm thick Co–Cr–Mo prosthesis located at a depth of 8 cm, the dose correction factors calculated at a distance 10 cm beyond it are 0.68 and 0.78, producing an attenuation of 32% and 22% for incident 6 and 18 MV clinical photon beams, respectively. If the linear attenuation coefficient method is used, Eq. (4) yields an attenuation of about 37% and 28% for 6 and 18 MV photons, respectively. The effective TMR method gives less attenuation because it includes a scatter contribution. These correction methods do not take into account the dimensions of the prosthesis relative to the field size or the position of the prosthesis relative to the point of calculation. Two other approximate methods that partly account for the location of the prosthesis are the Batho correction and a substraction technique described by Khan[63] which is similar to estimating the dose behind a block in a radiation field.

In regions of electronic disequilibrium, which exist within $d_{\max}$ of the prosthesis, the previously discussed simple dose correction methods are not applicable. Here, the dose may be estimated using Eq. (3) and Tables I and II that provide measured values for BSDF and the FDPF for metal slabs as a function of distance from them for 6 and 18 MV photon beams. For dose estimates near steel and titanium, Fig. 2 (Ref. 56) may be used.

b. Treatment planning calculations. The effect of a hip prosthesis on the absorbed dose in a patient with prostate cancer and a Co–Cr–Mo hip prosthesis is illustrated in Fig. 5. Isodose distributions, both uncorrected and corrected (using the TMRs ratio method for heterogeneity corrections) for the presence of the prosthesis, are shown. The target volume (shaded area) represents the prostate plus margin. The plan consists of 48.6 Gy tumor dose delivered with a 10 MV x-ray four-field "box" technique and a boost of 18 Gy delivered with 10 MV x-ray, 120° bilateral arcs. Using the water-equivalent depths with the ratio of TMRs and the appropriate electron density for the prosthesis, the isodose distributions can be calculated to within 3% to 5% when compared to measurements in a heterogeneous phantom at distances beyond the regions of interface effects.[14,17] To obtain a treatment plan with heterogeneity corrections, it can be contoured, or if the treatment planning system allows, a voxel by voxel inhomogeneity correction using CT numbers can be made. The problem is that the CT number to electron density conversion factor may not account for the high-Z inhomogeneity and there are also image artifacts. Usually the system allows for auto contouring by seeking the difference between the densities of different structures. This will lead to several problems due to artifacts produced on the CT image. However, either the CT or simulation film images should be satisfactory for determining the outer dimensions of the prosthesis. The problems have been discussed along with possible solutions by Alecu *et al.*[64] and are discussed further in Sec. IV B 1 *d*. The accuracy of the manual contouring process can be increased by adjusting the contrast levels on each CT slice as illustrated in Fig. 4(d). Due to these effects the CT number, and therefore the electron density of the prosthesis, cannot be accurately determined by the treatment planning algorithms. If the type of the prosthesis is known, the electron density can be obtained from Table III. If the type of prosthesis is unknown, the electron density can be estimated by making an approximate measurement of the attenuation coefficient in the megavoltage beam (see Sec. IV B 1). When the option to correct for tissue heterogeneity is chosen, the algorithm may correct for the presence of all areas having a CT number different from water. If the algo-

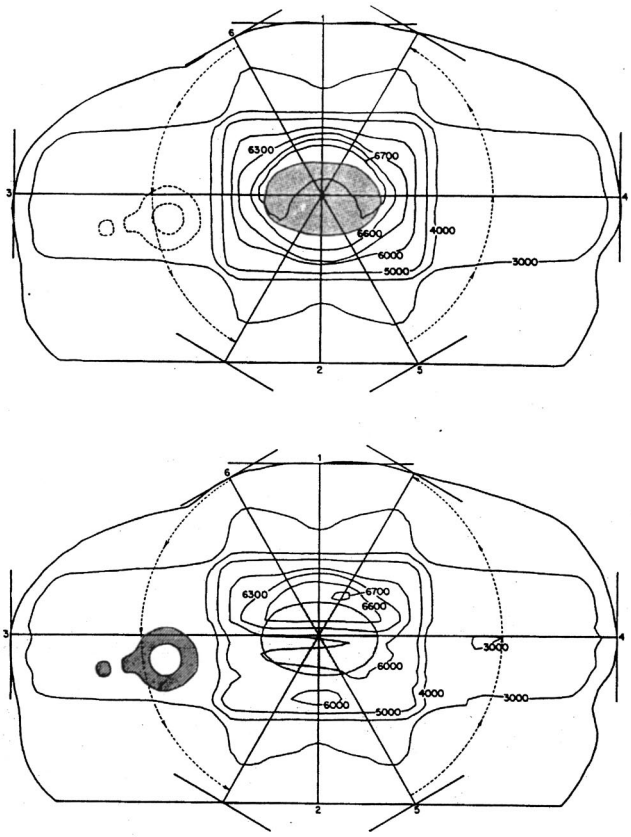

FIG. 5. Prostate treatment plan using 10 MV photons for a patient with a single hip prosthesis 48.6 Gy using four-field box technique followed by 18 Gy boost with 120° bilateral arcs. Upper treatment plan with no inhomogeneity correction, and the lower plan using a TMR method [see Eq. (5)] of heterogeneity correction (reprinted from Ref. 14).

TABLE VII. Monitor units to deliver 2 Gy dose at isocenter with equally weighted 18 MV beam using homogeneous, 2.5D and 3D calculation methods.

Calculation	Anterior	Posterior	Right	Left
Homogeneous	57	56	70	69
2.5D	58	59	80	133
3D	58	58	79	126

rithm allows, the user should correct only for specific inhomogeneities.

The CT images cannot show whether the prosthesis is hollow or solid because the low-energy x rays used in CT do not penetrate the metallic part of the prosthesis. If information from the manufacturer is not available to determine if the device is solid or hollow, portal imaging with the treatment beam should be performed. If the prosthesis is hollow, the dimensions and geometry of the air cavity can be estimated from an orthogonal pair of portal images and then drawn manually on each slice within the prosthetic head. In this situation the TPS should correct for both heterogeneities: metal and the air cavity. It is the responsibility of the medical physicist to determine how accurately the treatment planning system accounts for high-Z materials. Measurements in a water-equivalent phantom similar to those described by Roberts[10] can be performed to test the accuracy of the system to account for high-density materials. Alternatively, if the composition of the prosthesis is known, the dose calculated by the TPS for a single beam passing through the prosthesis can be compared to that calculated using Eq. (4) or (5). This procedure only needs to be done once, like other tests made in commissioning the TPS.

c. Dose distribution comparison for three different modes of computing does. Here we give an example of the differences in dose distribution and in monitor units (MUs) for the treatment of the prostate using a four-field "box" plan for a patient with a solid steel implant for a left femur replacement. All beams are 18 MV and are equally weighted to give a total of 2.0 Gy to the isocenter. The dose is computed using convolution/superposition algorithm system (Pinnacle, Version 4.2F) in three different modes:

(1) assuming that the patient is homogeneous water (1D calculation),
(2) assuming that the scatter is distributed in space as if the patient was homogeneous, while the primary is computed correctly, observing the spatial distribution of densities (2.5D convolution calculation), and
(3) both primary and scatter components incorporate the distribution of densities in the dose calculation (density scaling is an approximation since the implanted Z is nonwater equivalent) and performing a 3D superposition calculation using the collapsed cone convolution algorithm, where convolution kernels are scaled by the mass density of the patient (O'Connor's theorem).

Table VII gives the MUs for the three modes of dose calculation for a patient. The increase in MUs for the right field for methods 2 and 3 is due to the presence of bone. The MUs for the left field rise sharply as the density of the implant is included in the calculation. In fact the 3D calculation predicts a slightly lower value than the 2.5D calculation. This is attributed to the differences between the two mechanisms to account for the scatter distribution as described earlier. However, if MUs are adjusted to account for attenuation through the prosthesis, hot spots of the order of 20% may occur in the normal tissue, which could be unacceptable for the patient treatment.

d. Methods to minimize artifacts from a metal prosthesis on CT images. Methods to overcome the problems caused by high atomic number materials by improving image reconstruction and dose calculation methodology have been published,[65–69] although, as yet, none are commercially available. The standard method of image reconstruction, filtered back projection, gives characteristic streak artifacts due to aliasing when attempting to create images from patients containing high-Z materials. The loss of diagnostic quality and corrupted density information is illustrated in Fig. 4(c). Several attempts to overcome this limitation have been made in the past.[68,69] Besides aliasing scatter, low signal-to-noise-ratio behind the prosthesis, beam hardening, or any other phenomenon that makes CT detector response to attenuation nonlinear will degrade the image.

Future developments including megavoltage imaging using tomotherapy or cone beam reconstructions or more robust numerical algorithms may help produce streak-free images. In selecting a CT scanner for purchase, you should consider the availability and support for artifact reduction algorithms.

2. Current TPS limitations and future possibilities

The physicist should be aware that not all commercially available TPSs allow for adjustment or manual input of CT numbers. Also, some systems have an upper limit for the electron density used for the heterogeneity correction algorithm. Table VIII provides information on some commercially available TPS regarding heterogeneity correction algorithms and their flexibility. This table provides a snapshot of the capabilities of TPS at this time. The medical physicist should consult with the commercial vendors to determine the latest capabilities of their TPS. From the data in Table VIII, all but one system allows to some degree the editing of CT numbers and electron densities. Some groups have published[9,69] a comparison of the results of Monte Carlo simulations to the calculations with a commercial TPS of the dose perturbation produced by a prosthesis. An illuminating discussion on the differences between measurements and treatment planning calculations is given by Roberts.[10] He showed using one particular type of dose calculation that the accuracy of dose calculation varies with beam energy and depth (e.g., behind a steel prosthesis the pencil beam algorithm overestimates the dose by 11% and 15% for 6 and 15 MV photons, respectively). This work illustrates the kind of quality assurance the medical physicist should perform to understand the limitations of their TPS.

TABLE VIII. Characteristics of commonly used treatment planning systems obtained from the manufacturers in 2001. For more recent information contact the manufacturers.

TPS, code and version	Algorithm	Allows for editing of CT no.	Upper limit of allowed CT number (in Hounsfeld Units) or density
ADAC Laboratories version 4.2f	Adaptive collapsed cone convolution superposition, v.4.2f	Yes	Practical limit on density is 12 g/cc
CMS Focus 2.40	(a) Clarkson (effective pathlength) (b) FFT convolution kernels (not scaled but beam hardening accounted for)	Yes	No upper limit
CMS Focus 2.5.0 and later	Multigrid superposition (convolution kernels scaled with density)	Yes	15 (relative electron density)
LLNL Peregrine first release Distributed by NOMOS	Full 3D Monte Carlo code based on cross sections of photon interactions with inhomogeneities at the atomic level	Yes	No limits CT no. can be set to actual or negative as a key for change in calculation model
MDS Nordion THERAPLAN Plus v3.5	Equivalent TAR plus electron transport	Yes. Contour voxels are assigned bulk density.	No upper limit on CT number. No practical limit on density.
MDS Nordion Helax-TMS Version 6.0	(1) Fluence distribution engine: total, including a full head scatter model of all beam collimating and modifying elements. (2) Energy transport engines: • pencil kernel with depth scaling • collapsed cone point kernel with 3D scaling	Yes	CT nos.: No upper limit of CT values. However, CT values above 2832 in HU units are considered to be induced by stainless steel implants. Manually assigned densities: No upper limit.
MDS Nordion Oncentra DM (Dose Modeling) Module v1.0A	(1) Fluence distribution engine: total, including a full head scatter model of all beam collimating and modifying elements. (2) Energy transport engines: • pencil kernel with depth scaling • collapsed cone point kernel with 3D scaling	No. DM is a calculation server with no user interface for modifying contour density values. This would have to be done on originating system (e.g. CT Sim, VSIM)	CT numbers: No upper limit of CT values. However, CT values above 2832 HU units are considered to be induced by stainless steel implants.
Medtronic Sofamor Dainek. ARTS 3D 2.1	ETAR (equivalent TAR)	No, but will be added in the future release.	No upper limit
Nucletron: Plato RTS 3D 2.3	**3D Dose algorithm**: Bortfeld's method of pencil beam/convolution (Ref. 89) **Heterogeneity Correction**: Sontag and Cunningham's (Ref. 90) equivalent TAR method applied by Yu and Wong (Ref. 91)	Yes.	No upper limit
ROCS, 5.0	Equivalent path length and TMR ratio	No	±1000 HU
Varian, Cadplan	Pencil beam convolution User's choice: (a) equivalent TAR (b) Batho power law (c)Modified Batho power law	Yes	2000 HU

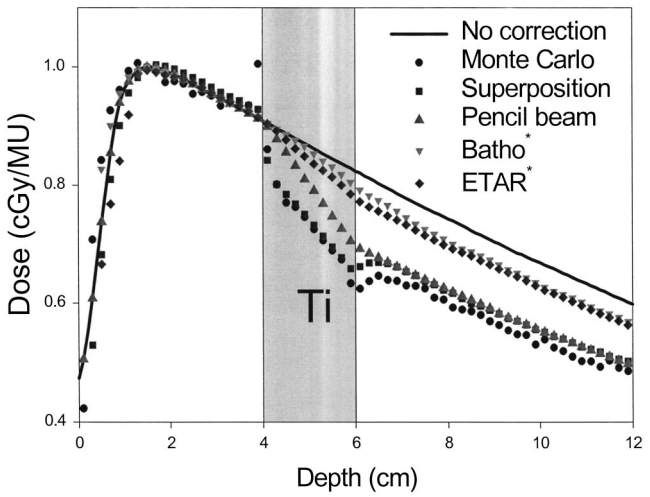

FIG. 6. A comparison of Monte Carlo calculated central axis depth dose with superposition, pencil beam, Batho, and ETAR calculation algorithms for a 6 MV beam incident on a water phantom containing a $2\times2\times2$ cm^3 titanium implant. Note that the Batho and the ETAR calculations shown in the figure were performed on a TPS with an upper limit for the implant density of 3.0 g/cm^2.

An obstacle to accurate dose calculations is the high-Z image reconstruction limitations discussed in Sec. IV B 1 *d* Once the image reconstruction algorithms are developed to support quantitative CT attenuation measurements of dense metal objects and artifact-free soft-tissue imaging, an accurate method of transporting particles is needed which accounts for the density and composition of the implant. Current commercial algorithms, both correction and model based, are unable to accurately predict the dose near high atomic number implants. The Monte Carlo methods[70–72] are well suited to this application as individual particles are transported, with the relevant interaction cross sections being taken from the media through which the particles are being transported. Although Monte Carlo methods for radiotherapy dose calculation may soon become a clinical reality, the correction- or model-based TPS will still be used in most clinics in the near future.

To illustrate the magnitude and extent of the dosimetric effects of a high-Z implant, a central axis depth dose curve in water calculated by the Monte Carlo (EGS4/BEAM)[73,74] method for a 6 MV beam incident on a water phantom containing a $2\times2\times2$ cm^2 implant is shown in Fig. 6. The complexity of the dosimetric effects is not accounted for by any of the other methods currently available. Depth dose curves calculated with some commonly used algorithms are compared to the Monte Carlo results in Fig. 6. Monte Carlo is the only algorithm that predicts the large increase in dose near the proximal water–titanium interface. The Batho and ETAR calculations performed here were obtained with a TPS with an upper density limit of 3.0 g/cm^3, and thus overestimate the dose distal to the implant. Hence it is not only important to have accurate dose calculation algorithms, but also the ability to assign the correct density to the implant. This point was emphasized by Roberts,[10] who reported similar results on the importance of using the correct density for the implant in the dose calculation, and thus the ability to edit CT images is an important feature of a TPS.

3. Neutron production

Photon beams with energy higher than 10 MV are contaminated with neutrons from the accelerator head. Neutrons are also created inside patients irradiated with these high-energy photon beams. The general conclusion from various reports[75,76] on this subject is that the neutron dose to patients undergoing typical high-energy photon irradiation therapy is negligible compared to the photon dose. Due to the interaction of these neutrons after thermalization with the metallic prosthesis, there exists a potential for increased photon dose around the device.[77] The following calculation provides an estimate of the additional photon dose resulting from (n, γ) reactions in patients with hip prostheses to indicate the magnitude of the effect.

The solid head of a titanium-based prosthesis can weigh as much as 500 g. The cross section for thermal neutron capture for Ti is 9 barns (9×10^{-24} cm^2). Ti-48 was chosen for this calculation because it is the most naturally abundant isotope. The head of the Ti prosthesis at approximately 5 cm depth inside a patient will be exposed to about 2.37×10^6 n/cm^2/s (100 cm SSD) when irradiated by an 18 MV photon beam[77] at 400 MU/min. The neutron flux may be higher or lower depending on the type of accelerator and the irradiation setup.[75–77] Thermal neutron capture will result in prompt gamma-ray emission with an average energy of 3.30 MeV. The dose rate due to these prompt gamma rays is about 0.74 cGy/min at 1 cm distance from the implant. These calculations assume that the photons originate from a point source of Ti weighing 500 g, that is, any self-absorption of these high-energy photons inside the metal is ignored and therefore can be considered a conservative estimate. Knowing the dose rate of the linear accelerator (at least 200 cGy/min) and the dose delivered by the beam passing through the prosthesis, one can estimate that the extra neutron induced photon dose is less than 0.5% of the photon dose at 1 cm from the prosthesis, and, therefore, can be assumed to be clinically negligible.

C. *In vivo* measurements

There are many types of prostheses with variations in composition (relative electron density), as previously discussed. Often, detailed information on the type of prosthesis in a particular patient is not available and hence dose calculations will have large uncertainties. For these situations, *in vivo* measurements can be useful to help determine the effective composition of the prosthesis and differentiate Ti from steel or Co–Cr–Mo. These measurements in combination with image reconstruction information described in Sec. IV B 1 *b* can be used to estimate the target dose.

The most conclusive type of measurement is an intracavitary one obtained during the patient irradiation. Two groups[15,16] describe *in vivo* TLD measurements in patients with hip prostheses. In these patients catheters loaded with TLDs were inserted in a urological catheter placed into the

bladder and irradiated during part of a treatment session. The location of the TLDs with respect to the patient's anatomy was verified using metal markers. The results of the TLD measurements of Burleson *et al.*[17] showed a 10% to 15% dose reduction for a conventional four-field beam geometry in a patient with bilateral total hip replacement prostheses. Hazuka *et al.*[15] compared their *in vivo* TLD results with heterogeneity corrected dose calculations using the ratio of the TMR correction algorithm, and an estimated thickness of the prosthesis from CT. The difference between the measured and calculated doses was only 3%. Unfortunately, their TLD calibrations had a rather large error (8.3%, 1 SD). An obvious limitation of this type of *in vivo* measurement is the added inconvenience and discomfort for the patient, and is unlikely to be performed. Instead, *in vivo* dosimetry using detectors positioned on the skin of the patient and at the exit surface of the beam is often used as a method to assess the dose inside the patient.[78–81] Many exit dose measurements relating to hip prostheses described in the literature are performed with diodes. However, thermoluminescent detectors (TLDs) and film have also been used. If film is used, a calibration curve for the particular type of film should also be obtained. Those interested in performing these types of measurements should consult the ESTRO booklet[82] which provides a comprehensive literature review on the clinical use of both diodes and TLDs and an ESTRO publication[83] on performing *in vivo* dosimetry with a diode.

The exit dose for the beam passing through prosthesis is calculated from a detector reading using the equation

$$D_e = R \times K \times II_i C_i , \tag{7}$$

where D_e is the exit dose, R is the detector reading, K is the detector calibration factor measured under reference conditions,[77–81] and $II_i C_i$ are a product of correction factors for the different detectors under nonreference irradiation conditions. These C_i factors are related to the type of detector. For example, ionization chambers will have corrections for recombination and temperature and pressure, diodes will have corrections for dose rate and angular response, and film may have corrections for scattering conditions. The subscript, e, refers to the actual measurement condition for measuring the exit dose. The attenuation of the beam produced by the prosthesis at a point along a given ray can now be obtained by calculating the transmission through the prosthesis as a ratio of the exit dose measured in the shadow of the prosthesis and the dose at the same point, calculated by the TPS, for a homogeneous case (neglecting the presence of the prosthesis). The attenuation estimated in this way, at the exit surface, is 2% to 6% lower than the actual broad beam attenuation depending upon the energy, patient separation, and field size. This is because internal scatter will partially cancel the attenuation effect of the prosthesis at distances distal to the inhomogeneity. This is a small effect compared to the attenuation introduced by the prosthesis in the target volume. The accuracy of *in vivo* dosimetry is very dependent on the immobilization of the patient and the accurate positioning of the patient and detector. However, exit dose measurements can provide an estimate of the error in TPS calculations, if the heterogeneity correction option is activated.

A drawback of *in vivo* dosimetry using diodes or TLDs is that the dose is only measured at a limited number of points instead of over the shadow of the target. One method to obtain spatial dose information is to use film as described by Van Dam *et al.*[84] A promising approach is to use the information in a portal image to verify the dose calculation. Relative dose distributions transmitted through the patient, obtained with a portal image, can be used to determine the radiological path length through the prosthesis. This can be done by measuring dose profiles through the projection of the prosthesis after converting the optical density of a film, or the pixel values of an image of an electronic portal imaging device, into dose values.[85] The resulting reduction in transmission at the position of the prosthesis, compared with adjacent values, can then be converted into a radiological path length that can be used for dose calculation as illustrated in Figs. 7(a) and 7(b). Currently, several groups have developed methods[85–87] to relate the information in the portal image directly to the dose distribution in the patient. However, these methods are still evolving and slowly coming into clinical use, and the rather complicated algorithms for patient dose calculations are not yet widely available. Therefore, in the near future, only the simple relative methods described previously are likely to be available for clinical needs.

V. POSSIBLE ACTIONS FOR MINIMIZING THE DOSE PERTURBATIONS

Perturbations of the dose distribution by a hip prosthesis when treating pelvic malignancies can result in unacceptable dose inhomogeneities within the target volume. Such an inhomogeneous dose distribution may compromise local control and, therefore, beam arrangements to completely or partly avoid the prosthesis (e.g., avoid using or reduce the weight of the lateral beam on the side of the prosthesis or consider using rotational fields) have been proposed, and are often the preferred solution. Sometimes these techniques are not the best choice since the dose to organs at risk may be unacceptably high. Tolerance doses to normal tissue can be found in the literature.[59] Therefore, alternative methods to compensate for the beam attenuation due to the prosthesis may be more suitable. In determining a course of action, it is important to consult closely with the radiation oncologist regarding the treatment goals. For patients treated to a low prescription dose, the dose perturbation caused by one of the fields traversing part or all of the prosthesis may still produce a clinically acceptable isodose distribution in the normal tissue. Alternatively, a simple heterogeneity correction to adjust the treatment MUs may provide an acceptable plan. In either case the normal tissue consequences of either changing the beam arrangements or giving more MUs through the prosthesis are reduced for low treatment doses. However, patients treated to a high prescription dose may require a more sophisticated treatment plan. In particular, due to the uncertainty in the dose calculations near a high-Z material, there is

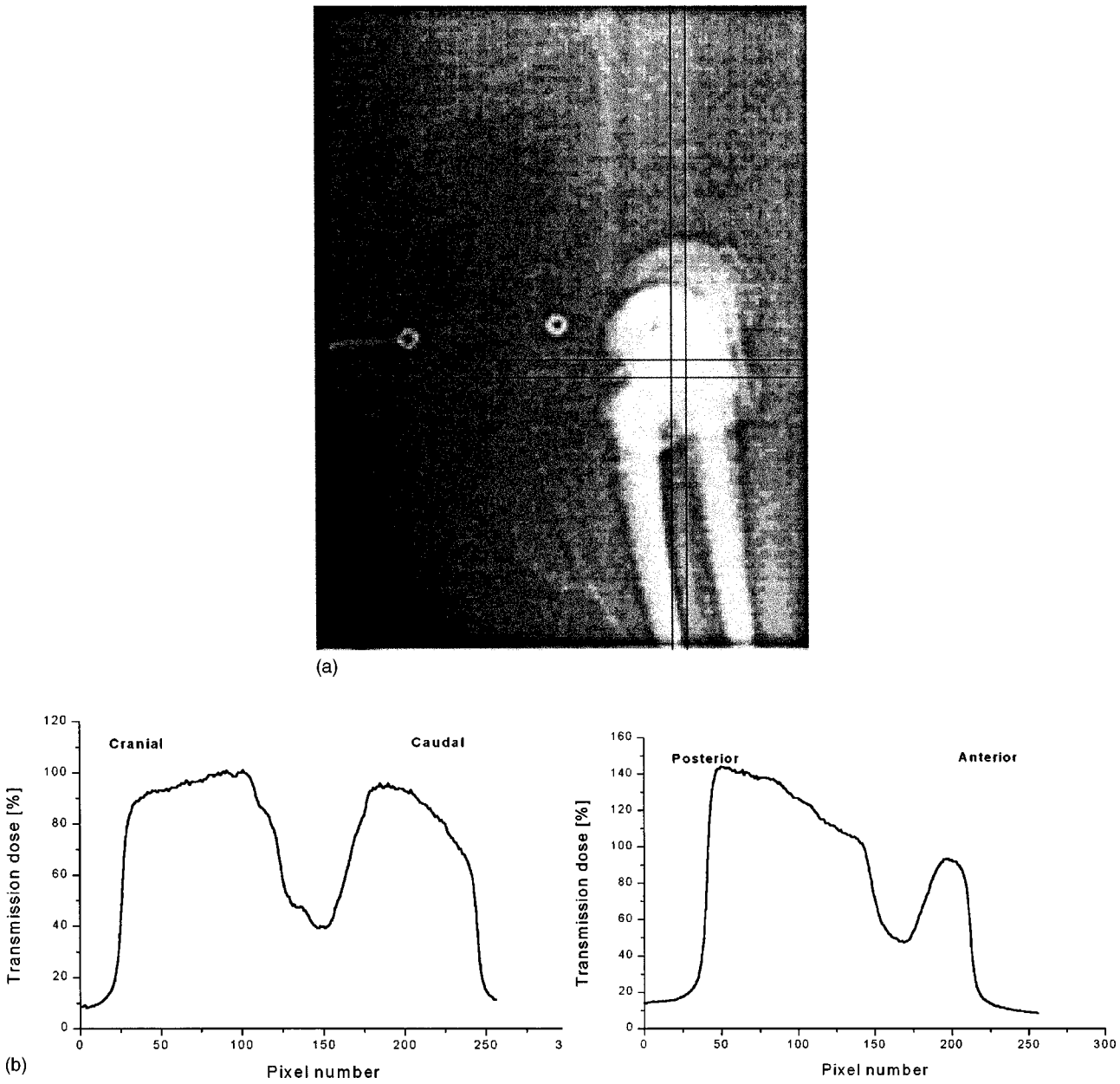

FIG. 7. (a) Portal image of a patient having bilateral hip prostheses. (b) Relative dose distribution along the lines indicated in the portal image.

the potential of increased bone necrosis, especially for patients undergoing dose escalations. A possible solution for their treatment planning is to assure that, within a 1 cm thick rind of tissue around the prosthesis, the maximum dose calculated by the TPS is below 55 Gy. This would allow for a possible 15% increase in dose to the bone from interface effects and maintain the normal tissue complication probability dose for the femoral head of 65 Gy (TD 50/5—the probability of 50% complication within 5 years[59]).

A. Special beam arrangements

As previously mentioned, the first option to consider when treating a patient with a metal prosthesis is to design a treatment plan with beams that do not pass through the device. Although this method avoids the dosimetric complications of the metallic inhomogeneity, it may result in compromising the patient treatment by increasing the dose to organs at risk. The following example illustrates this point. For treating patients with prostate cancer, while avoiding the prosthesis, numerous treatment techniques have been developed.[27,28] One of the most commonly used techniques is four oblique fields or "diamond" plan. A comparison of the standard four-field "box" plan with the "diamond" plan is made for treatment with 18 MV photon beams using Render Plan 3D TPS. Dose-volume-histograms (DVHs) were calculated with the same target volume planned for these two techniques. Table IX summarizes the DVH results. The rectal dose and bladder dose are significantly higher with the "diamond" technique. These results will vary depending upon the anatomy of the patient and the extent of the disease, as discussed by Agapito.[27]

TABLE IX. Summary of DVHs.

	Four field box	Diamond
Rectum	100% Vol≥50% Dose	100% Vol≥50% Dose
	38% Vol gets 100% Dose	99% Vol gets 100% Dose
Bladder	60% Vol≥50% Dose	77% Vol≥50% Dose
	8% gets 100% Dose	36% Vol gets 100% Dose
	19%≤20% Dose	16% Vol≤20% Dose

Examples of alternate beam arrangements to avoid treating through a hip prosthesis are presented. One technique for treating cancer of the prostate involves six high-energy photon beams: two opposed lateral fields and two pairs of opposed oblique fields. Figure 8(a) shows the central axis isodose distribution without inhomogeneity correction for 18 MV photons for six fields superimposed on a transverse CT cut through the prostate. To avoid the prosthesis three different treatment plans were developed for this patient: a five-field plan [Fig. 8(b)], a five-field plan with wedges [Fig. 8(c)], and a three-field plan with wedges [Fig. 8(d)]. These plans are provided as examples of treatment options that avoid the metallic prosthesis. The optimal plan for covering the target and minimizing the dose to the critical structures depends upon the patient anatomy and the extent and location of the disease. To compare the plans the integral DVHs are shown in Fig. 9. All the plans completely cover the target, but there are significant differences in the dose to the rectum and bladder among these three plans. Although the DVH for the three-field plan shows significant sparing of the rectum, this must be weighed against the increased dose to the right femoral head illustrated by the isodose distribution in Fig. 8(d). In appropriate cases more complex non-coplanar beam arrangements may be considered. However, these should be weighed against the practical issues such as ease of treatment planning and delivery, gantry-couch collision, portal verification, and staff training. Therefore, the advantages and disadvantages of modified treatment techniques to avoid dosimetric complications should be carefully considered and discussed with the radiation oncologist.

B. Dose compensation

There are two general methods to correct for the effect of a prosthesis on target dose distribution. In one method forward planned intensity modulated beams are used to compensate beams that traverse the prosthesis while in the other method inverse planned intensity modulated beams are used to provide normal tissue protection and target coverage with beams that avoid the prosthesis. In the former method two dose compensation techniques have been reported by Alecu *et al.*[64] The first technique uses a traditional compensator. The other uses manually created intensity modulated x-ray beams using a multileaf collimator. In the first method the dose information available from a portal image is taken to construct a physical compensator filter. A limitation of such a compensator system is that it cannot be used for patients with bilateral hip prostheses. This problem may be overcome with the second method. A dose compensator is designed

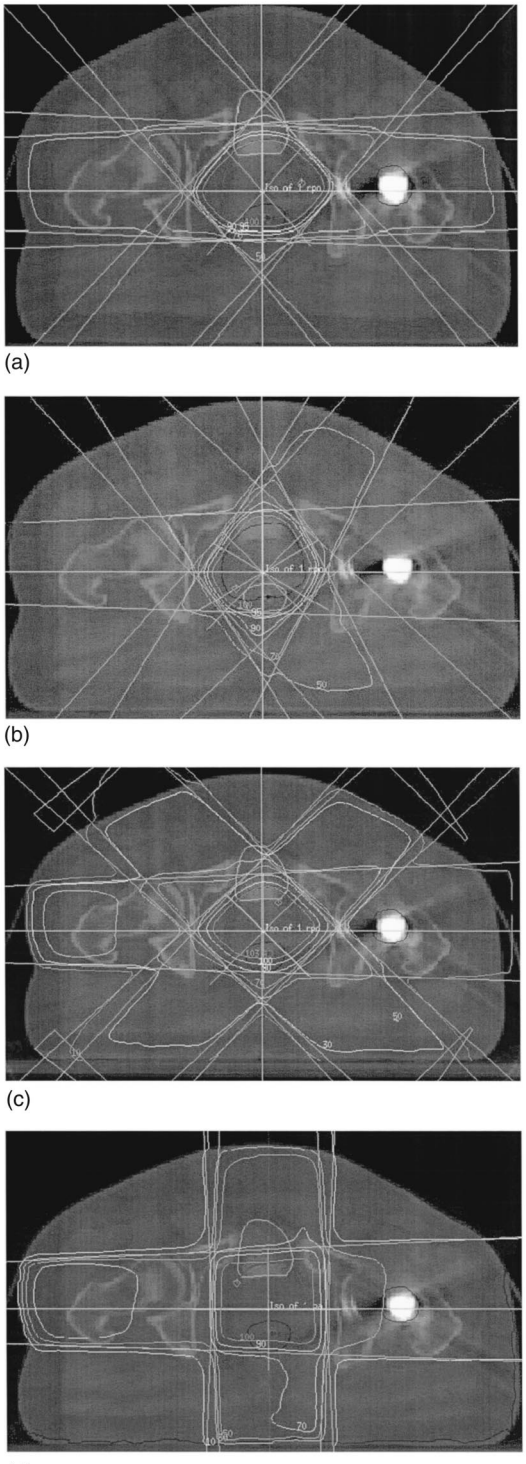

FIG. 8. (a) Transverse isodose distribution through the central axis for a six-field plan: Two opposed lateral fields and two pairs of opposed oblique fields using 18 MV photons. The following three field arrangements are designed to avoid the prosthesis. (b) Five-field plan: two anterior oblique fields, two posterior oblique fields and a right lateral field for 18 MV photons. (c) A five-field plan with wedges: two anterior oblique fields, two posterior oblique fields, and a right lateral field for 18 MV photons. All of the oblique fields have a 30° wedge. (d) A three-field plan with wedges: 6 MV anterior field with a 45° wedge, 18 MV posterior field with a 30° wedge, and 18 MV right lateral field with a 15° wedge. In all of these plans the field sizes are adjusted to conform to the target and the dose distributions are obtained with PLUNC, Plan University of North Carolina, 3D treatment planning system.

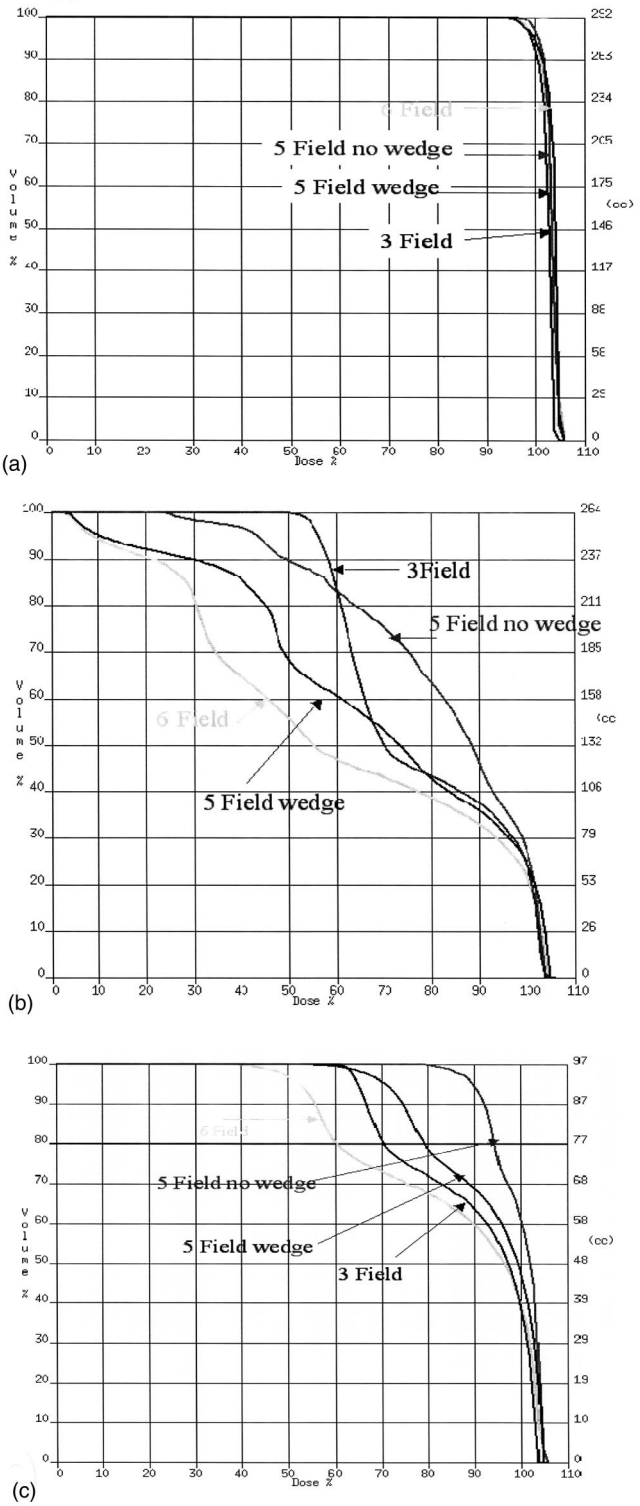

FIG. 9. Summary of the dose volume histograms for the target, bladder, and the rectum for the four different treatment techniques as shown in Figs. 9(a)–9(d).

using a CT simulation, 3D treatment planning, and multileaf collimators to produce segmental fields that allow high intensity over the prosthesis. These methods of dose compensation produce a high dose perturbation in the normal tissue upstream of the prosthesis, which should be evaluated. These techniques require accurate characterization of the prosthesis geometry, accurate dosimetry modeling in the presence of the metallic implant, as well as good patient immobilization and accurate registration of the compensator to the patient. Precautions similar to those in treatment planning should be taken for the design of the compensator. Additionally, *in vivo* measurements should be performed to verify its accuracy. Because of these factors and the labor involved in designing and constructing the compensators (less labor is involved using a multileaf collimator), they will probably be of limited use in a busy clinic that does not have the necessary physics and technical support.

An example of the latter method is intensity modulated radiation therapy (IMRT) with dynamic multileaves as in the step-and-shoot method in combination with inverse treatment planning. This treatment modality is becoming more available and potentially offers better treatment plans for the prostate. By making the prosthesis a critical structure to avoid or choosing beams that avoid it, treatment plans can be developed using inverse treatment planning techniques[88] that are comparable to the commonly used six-field technique. Alternatively, to provide more flexibility in developing treatment plans, the prosthesis can be selected as a critical structure with a dose constraint. One study[88] compares conformal six-field and five-field plans with a nine-field IMRT plan. As an example, Fig. 10 shows the comparison of DVHs for the bladder, rectum, and PTV for a five-field 3D conformal 18 MV plan and a nine-field 6 MV IMRT plan for a patient with a prosthesis. A six-field 18 MV plan with the inhomogeneity correction turned off is shown as a reference for comparison. The IMRT plan compares favorably with the reference plan.

VI. RECOMMENDATIONS

This Task Group recommends the following protocol:

(1) Find out from your treatment planning system manufacturer the possibilities and limitations regarding heterogeneity corrections for high electron densities of the treatment planning algorithm available within your department. Determine and test if electron densities can be changed in user-selected regions, if there is an upper limit to this value and how to edit the streak artifacts (see Table VIII and Sec. IV B 1 *b*). Verify this information with some phantom measurements such as those described by Roberts[10] or with hand calculations.

(2) The radiation oncologist should inform the physicist in advance if a patient with a hip prosthesis is scheduled to be simulated for pelvic radiation.

(3) Beam arrangements that avoid the prosthesis should be considered first, and this option should be discussed with the radiation oncologist.

(4) If the decision is made to use a technique with beams which avoid the prosthesis, the following additional steps are recommended:

4.1 Use standard immobilization and simulation or CT simulation.

4.2 Perform treatment planning. Check with the simulator films and/or DRRs that the prosthesis does not

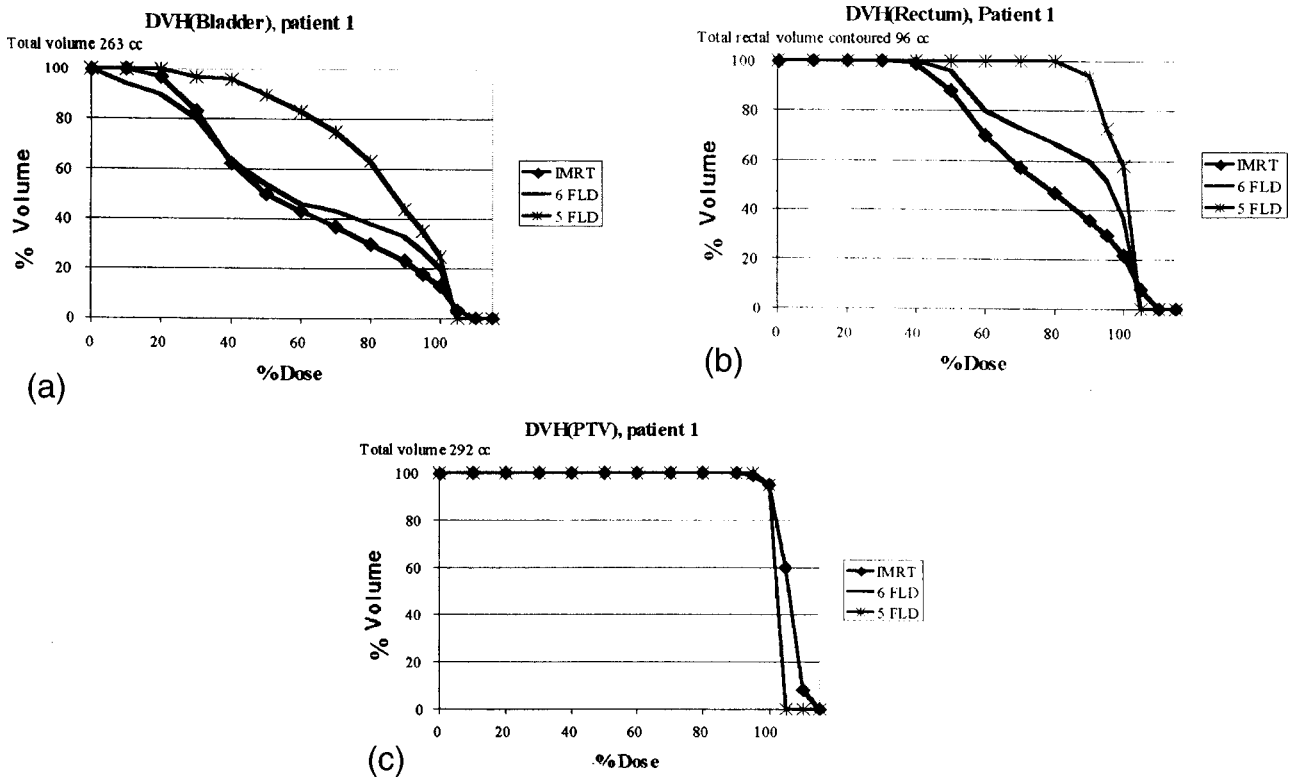

FIG. 10. DVHs for the bladder (a), rectum (b), and PTV (c) comparing five-field 3DCRT and IMRT plans. The six-field 3DCRT DVHs are shown for comparison. The conformal plans obtained with PLUNC (Plan University of North Carolina) and the IMRT plan obtained with CORVUS inverse treatment planning system.

shadow part of the target volume. For CT planning you can edit out the streak artifacts and turn off the inhomogeneity correction.

4.3 Take a port film or EPID image before or during the first treatment to verify that the prosthesis does not shadow part of the target volume.

(5) If treatment through the prosthesis is considered, then the following are recommended.

5.1 Discuss with the radiation oncologist the treatment plan for this patient. Include such questions as:

5.1.1. Is the patient getting a high or low target dose?

5.1.2. Is the dose to the bladder, rectum, or hip of concern?

5.1.3. What uncertainty in the target dose is acceptable?

5.2. Obtain before simulation as much data as possible about the prosthesis from the patient's medical records, the surgeon, and/or prosthesis manufacturer.

5.3. Inform the radiation oncologist about the approximate magnitude of the relevant dose perturbation and the capabilities of your TPS to make the corrections.

5.4. If the type of prosthesis is known, then the following steps are recommended:

5.4.1. Obtain the physical characteristics such as its dimensions from orthogonal simulator films or CT scouts, electron density (to use in planning, if necessary), approximate attenuation of the beam passing through the prosthesis, and possible dose increase to the hip bone, etc. from this report or other sources.[12,14]

5.4.2. Perform treatment planning (computerized isodose distributions with heterogeneity corrections, inputting the electron density). Use the most physically rigorous dose calculation algorithm available in your TPS.

5.4.3. Use published data on prosthesis attenuation and electron densities to compare your hand and treatment planning calculations.

5.4.4. Treat the first fraction based on 5.4.1 and take portal images and confirm whether the prosthesis is hollow or solid.

5.4.5. During the first fraction perform exit dose measurements with diodes, films, or TLDs to confirm and, if necessary, modify your treatment planning calculations and input characteristics.

5.5. If there are no data available on the physical characteristics, but the composition of the prosthesis is known, perform phantom measurements or a calculation for the attenuation (see Sec. IV B 1 *a*) and continue through steps 5.4.1–5.4.5.

5.6. If the type and characteristic of the prosthesis are unknown, then the following steps are recommended:

5.6.1. Perform treatment planning (computerized isodose distribution without heterogeneity corrections in order to calculate attenuation—Sec. IV B).

5.6.2. Check with the physician if films only (no treatment) can be taken on the first day to obtain information on the prosthesis. If not, treat the first fraction ignoring

the presence of the prosthesis based on 5.6.1.

5.6.3. During the first fraction:

5.6.3.1. Take port film or EPID and determine if prosthesis is solid or hollow.

5.6.3.2. Perform exit dose measurements with EPID, films, diodes, or TLDs (diodes will show up on portal films or EPID images).

5.6.4. Use these measured data to derive physical properties of the prosthesis, such as attenuation of the beam due to the prosthesis, which might allow you to identify the type of prosthesis and compare your results with published data.

5.6.5. Perform treatment planning (computerized isodose distribution with heterogeneity corrections) based on your calculated and measured data. Use the most accurate dose calculation algorithm available in your TPS.

5.6.6. During the second fraction perform exit dose measurements with detectors to confirm, and if necessary modify your treatment planning calculations and input characteristics. If the patient has more than 30 fractions, it might be acceptable to the physician for the patient to be treated with the original plan for the first few fractions while a more accurate treatment plan is developed.

5.7. Document the treatment plan and procedure used and inform the radiation oncologist about

5.7.1. The effect of the prosthesis on the target dose distribution and the uncertainty in estimating this effect,

5.7.2. The approximate magnitude of the interface effect, and

5.7.3. The possible increase in dose for organs at risk, peripheral tissue, etc.

Suggestions for future research work include the development of algorithms to reduce the streaking artifacts produced when reconstructing CT images of patients with prosthesis as well as algorithms to calculate accurately dose distributions near high-Z materials. Further study should also be performed on the biological effects of the increased tissue dose at the tissue-prosthesis interface.

ACKNOWLEDGMENTS

The Task Group members would like to thank Dr. George Ding for performing the ETAR and Batho calculations displayed in Fig. 6. We also would like to acknowledge the contributions to this report from Dr. Mary Hebert, Dr. Marius Alecu, Dr. Sam Beddar, and Dr. Radhe Mohan. Also, the Task Group is greatly thankful to Ellen Yorke for her very thorough reviews and constructive editing of the various versions during the drafting of this document.

[1] B. J. Mijnheer, "The clinical basis for dosimetric accuracy in radiotherapy," in *Radiation Incidents* (British Institute of Radiology, London, 1996), pp. 16–20.

[2] G. H. Fletcher, *Textbook of Radiotherapy* (Lea and Febiger, Piladelphia, 1981).

[3] ICRU 50 (ICRU Report 50), *Prescribing, Recording, and Reporting Photon Beam Therapy* (International Commission on Radiation Units and Measurements, Bethesda, MD, 1993).

[4] ICRU 62 (ICRU Report 62), *Prescribing, Recording and Reporting Photon Beam Therapy (Supplement to ICRU Report 50)* (International Commission on Radiation Units and Measurements, Bethesda, MD, 1999).

[5] TG-21, "A protocol for the determination of absorbed dose from high-energy photon and electron beams," Med. Phys. **10**, 741–771 (1983).

[6] TG-51, "AAPM's TG-51 protocol for clinical reference dosimetry of high-energy photon and electron beams," Med. Phys. **26**, 1847–1870 (1999).

[7] TRS No. 398, *Absorbed Dose Determination in External Beam Radiotherapy: An International Code of Practice for Dosimetry on Standards of Absorbed Dose to Water* (IAEA, Vienna, 2000).

[8] P. W. Grigsby, H. L. Roberts, and C. A. Perez, "Femoral neck fracture following groin irradiation," Int. J. Radiat. Oncol., Biol., Phys. **32**, 63–67 (1995).

[9] G. X. Ding and C. W. Yu, "A study on beams passing through hip-prosthesis for pelvic radiation treatment," Int. J. Radiat. Oncol., Biol., Phys. **51**, 1167–1175 (2001).

[10] R. Roberts, "How accurate is a CT-based dose calculation on a pencil beam TPS for a patient with a metallic prosthesis," Phys. Med. Biol. **46**, N227–N234 (2001).

[11] P. J. Biggs and M. D. Russell, "Effect of a femoral head prosthesis on megavoltage beam radiotherapy," Int. J. Radiat. Oncol., Biol., Phys. **14**, 581–586 (1988).

[12] C. H. Sibata, H. C. Mota, P. D. Higgins, D. Gaisser, J. P. Saxton, and K. H. Shin, "Influence of hip prostheses on high energy photon dose distribution," Int. J. Radiat. Oncol., Biol., Phys. **18**, 455–461 (1990).

[13] I. J. Das, K. R. Kase, A. S. Meigooni, F. M. Khan, and B. L. Werner, "Validity of transition-zone dosimetry at high atomic number interfaces in megavoltage photon beams," Med. Phys. **17**, 10–16 (1990).

[14] M. B. Hazuka, G. S. Ibbott, and J. J. Kinzie, "Hip prostheses during pelvic irradiation: effects and corrections," Int. J. Radiat. Oncol., Biol., Phys. **14**, 1311–1317 (1988).

[15] M. B. Hazuka, D. N. Stoud, J. Adams, G. S. Ibbott, and J. J. Kinzie, "Prostatic thermoluminescent dosimeter analysis in a patient treated with 18 MV x rays through a prostheic hip," Int. J. Radiat. Oncol., Biol., Phys. **25**, 339–343 (1993).

[16] F. R. Hudson, M. T. Crawley, and M. Samarasekera, "Radiotherapy treatment planning for patients fitted with prostheses," Br. J. Radiol. **57**, 603–608 (1984).

[17] W. D. Burleson, C. D. Stutzman, J. A. Stitt, U. L. Karlsson, and T. A. Mian, "In vivo isocenter dose in two hip prosthesis patients," Int. J. Radiat. Oncol., Biol., Phys. **20**, 1347–1352 (1991).

[18] M. Erlanson, L. Franzen, R. Henriksson, B. Littbrand, and P. Lofroth, "Planning of radiotherapy for patients with hip prosthesis," Int. J. Radiat. Oncol., Biol., Phys. **20**, 1093–1098 (1991).

[19] N. Scher, D. Poe, F. Kuchnir, C. Reft, R. Weichselbaum, and W. R. Panje, "Radiotherapy of the resected mandible following stainless steel plate fixation," Laryngoscope **98**, 561–563 (1988).

[20] M. H. Castillo, T. M. Button, R. Doerr, M. I. Homs, C. W. Pruett, and J. I. Pearce, "Effects of radiotherapy on mandibular reconstruction plates," Am. J. Surg. **156**, 261–263 (1988).

[21] R. R. Wang, K. Pillai, and P. K. Jones, "In vitro backscattering from implant materials during radiotherapy," J. Prosthet. Dent. **75**, 626–632 (1996).

[22] R. Wang, K. Pillai, and P. K. Jones, "Dosimetric measurement of scattered radiation from dental implants in simulated head and neck radiotherapy," Int. J. Oral Maxillofac Implants **13**, 197–203 (1998).

[23] D. P. Fontenla, M. Ahmad, C. S. Chui, B. McCormick, D. H. Abramson, and G. J. Kutcher, "Effect of occular implants of different materials on the dosimetry of external beam radiation therapy," Int. J. Radiat. Oncol., Biol., Phys. **32**, 1477–1480 (1995).

[24] T. J. Nelson and S. C. Sharma, "Irradiating with a prosthesis or metal pin in the radiation treatment field," Med. Dosim **13**, 113–118 (1988).

[25] P. M. Mondalek and J. M. Fayad, "Prostatic adenocarcinoma: treatment planning consideration with a hip prosthesis," Med. Dosim. **8**(2), 5–6 (1983).

[26] M. D. C. Evans, H. J. Patrocinio, L. Souhami, M. Tanzer, and E. B. Podgorsak, "Dosimetry of hip irradiation for prevention of heterotopic bone formation after arthroplasty," Int. J. Radiat. Oncol., Biol., Phys. **43**, 1161–1165 (1999).

[27] J. Agapito, "Radical radiation therapy for carcinoma of the prostate in patients with single hip prosthesis: A technique analysis using dose-volume histograms," Med. Dosim. **26**, 243–250 (2001).

[28] S. E. Schild, J. S. Robinow, H. E. Casale, L. P. Bellefontaine, and S. J. Buskirk, "Radiotherapy treatment planning for prostate cancer in patients with prosthetic hips," Med. Dosim. **17**, 83–86 (1992).
[29] T. Y. Eng, "Dose attenuation through a titanium alloy hip prosthesis," Med. Dosim. **25**, 7–8 (2000).
[30] E. Melian, M. Fatyga, P. Lam, M. Steinberg, S. P. Reddy, G. J. Petruzzelli, and G. P. Glasgow, "Effect of metal reconstruction plates on Cobalt-60 dose distribution: A predictive formula and clinical implications," Int. J. Radiat. Oncol., Biol., Phys. **44**, 725–730 (1999).
[31] I. J. Das and F. M. Khan, "Backscatter dose perturbation at high atomic number interfaces in megavoltage photon beams," Med. Phys. **16**, 367–375 (1989).
[32] O. A. Sauer, "Calculation of dose distributions in the vicinity of high-Z interfaces for photon beams," Med. Phys. **22**, 1685–1690 (1995).
[33] F. W. Spiers, "The influence of energy absorption and electron range on dosage in irradiated bone," Br. J. Radiol. **22**, 521–533 (1949).
[34] F. W. Spiers, "Dosage in irradiated soft tissue and bone," Br. J. Radiol. **25**, 365–370 (1951).
[35] E. R. Epp, H. Q. Woodard, and H. Weiss, "Energy absorption by the bone marrow of the mouse receiving whole-body irradiation with 250-KV x-rays or cobalt-60 gamma rays," Radiat. Res. **11**, 184–197 (1959).
[36] W. K. Sinclair, "The relative biological effectiveness of 22-MV x-rays, cobalt-60 gamma rays, and 200-kVp x-rays. Absorbed dose to the bone marrow in the rat and the mouse," Radiat. Res. **16**, 369–383 (1962).
[37] C. L. Wingate, W. Gross, and G. Failla, "Experimental determination of absorbed dose from x-rays near the interface of soft tissue and other material," Radiology **79**, 984–1000 (1962).
[38] S. L. Hood and G. Morris, "Dosimetry of human cell cultures irradiated at the interface in plastic and glass dishes," Radiat. Res. **14**, 705–712 (1961).
[39] N. Aspin and H. E. Johns, "The absorbed dose in cylindrical cavities within irradiated bone," Br. J. Radiol. **36**, 350–362 (1963).
[40] I. J. Das and K. L. Chopra, "Backscatter dose perturbation in kilovoltage photon beams at high atomic number interfaces," Med. Phys. **22**, 767–773 (1995).
[41] I. J. Das, "Forward dose perturbation at high atomic number interfaces in kilovoltage X-ray beams," Med. Phys. **24**, 1781–1787 (1997).
[42] H. Q. Woodard and J. S. Laughlin, "The effect of x-rays of different qualities on the alkaline phosphatase of living mouse bone," Radiat. Res. **7**, 236–252 (1957).
[43] J. Dutreix, A. Dutreix, and M. Bernard, "Etude de la dose au voisinage de l'interface entre deux milieux de composition atomique différente exposés aux rayonnement y du ^{60}Co," Phys. Med. Biol. **7**, 69–82 (1962).
[44] J. Dutreix and M. Bernard, "Dosimetry at interfaces for high energy X and gamma rays," Br. J. Radiol. **39**, 205–210 (1966).
[45] S. Webb, "The absorbed dose in the vicinity of an interface between two media irradiated by a ^{60}Co source," Br. J. Radiol. **52**, 962–967 (1979).
[46] B. L. Werner, I. J. Das, F. M. Khan, and A. S. Meigooni, "Dose perturbations at interfaces in photon beams," Med. Phys. **14**, 585–595 (1987).
[47] B. L. Werner, I. J. Das, and W. N. Salk, "Dose perturbations at interfaces in photon beams: secondary electron transport," Med. Phys. **17**, 212–226 (1990).
[48] B. J. Mijnheer, R. K. Rice, and L. M. Chin, "Lead-polystyrene transition zone dosimetry in high-energy photon beams," Radiother. Oncol. **11**, 379–386 (1988).
[49] I. J. Das. "Study of Dose Perturbation at Bone-Tissue Interfaces in Megavoltage Photon Beam Therapy," Ph.D. thesis, University of Minnesota, 1988.
[50] A. Niroomand-Rad, R. Razavi, S. Thobejane, and K. W. Harter, "Radiation dose perturbation at tissue-titanium dental interfaces in head and neck cancer patients," Int. J. Radiat. Oncol., Biol., Phys. **34**, 475–480 (1996).
[51] T. A. Mian, M. C. Van Putten, D. C. Kramer, R. F. Jacob, and A. L. Boyer, "Backscatter radiation at bone-titanium interface from high-energy X and gamma rays," Int. J. Radiat. Oncol., Biol., Phys. **13**, 1943–1947 (1987).
[52] V. Thambi, A. Murthy, G. Alder, and P. Kartha, "Dose perturbation resulting from gold fillings in patients with head and neck cancers," Int. J. Radiat. Oncol., Biol., Phys. **5**, 581–582 (1979).
[53] M. Murthy and A. Lakshmanan, "Dose enhancement due to backscattered secondary electrons at the interface of two media," Radiat. Res. **67**, 215–223 (1976).
[54] G. A. Carlsson, "Dosimetry at plane interfaces between a low Z-material and Al, Cu, Sn or Pb irradiated with 100 to 200 kV roentgen radiation. Theoretical analysis and measurements by means of thermoluminescent LiF," Acta Radiol., Suppl. **332**, 1–64 (1973).
[55] K. M. Stenson, J. M. Balter, J. H. Campbell, and C. R. Carroll, "Effects of implantable biomaterials on radiation dosimetry," Head Neck **19**, 384–390 (1997).
[56] P. J. Gullane, "Primary Mandibular reconstruction analysis of 64 cases and evaluation of interface radiation dosimetry on bridging plates," Laryngoscope **101**(6, pt. 2), 1–24 (1991).
[57] R. Nadrowitz and T. Feyerabend, "Backscatter dose from metallic materials due to obliquely incident high-energy photon beams," Med. Phys. **28**, 959–965 (2001).
[58] C. S. Reft and F. T. Kuchnir, "Dose correction factors at the bone-tissue interface for high energy photon beams," Med. Phys. **13**, 942 (1986).
[59] B. Emami, J. Lyman, A. Brown, L. Coia, M. Goiten, J. E. Munzenrider, B. Shank, L. J. Solin, and M. Wesson, "Tolerance of normal tissue to therapeutic irradiation," Int. J. Radiat. Oncol., Biol., Phys. **21**, 109–122 (1991).
[60] K. Shimanovskaya and A. D. Shiman, *Radiation Injury of Bone: Bone Injuries Following Radiation Therapy of Tumors* (Pergamon, New York, 1983).
[61] J. Kirchner and R. Bowman, *Effects of Radiation on Materials and Components* (Reinhold, New York, 1964).
[62] National Institute of Standards and Technology (NIST), www.physics.nist.gov/PhysRefData/XrayMassCoef
[63] F. M. Khan, *The Physics of Radiation Therapy*, 2nd ed. (Williams & Wilkins, Baltimore, 1994).
[64] R. Alecu, M. Alecu, T. Loomis, T. Ochran, and T. He, "Traditional and MLC based dose compensator design for patients with hip prostheses undergoing pelvic radiation therapy," Med. Dosim **24**, 33–37 (1999).
[65] G. Wang, D. L. Snyder, and A. O. O'Sullivan, "Iterative deblurring for CT metal artifact removal," IEEE Trans. Med. Imaging **15**, 657–664 (1996).
[66] R. L. Morin and D. E. Raeside, "Removal of streaking artifact in computed tomography," J. Med. Syst. **6**, 387–397 (1982).
[67] G. H. Glover and N. J. Pelc, "An algorithm for the reduction of metal clip artifacts in CT reconstructions," Med. Phys. **8**, 799–807 (1981).
[68] D. D. Robertson, J. Yuan, and G. Wang, "Total hip prosthesis metal-artifact suppression using iterative deblurring reconstruction," J. Comput. Assist. Tomogr. **21**, 293–298 (1997).
[69] P. Keall, L. Chock, R. Jeraj, J. Siebers, and R. Mohan, "Image Reconstruction and the Effect on Dose Calculation for Hip prostheses," Med. Dosim. (in press).
[70] D. E. Raeside, "Monte Carlo principles and applications," Phys. Med. Biol. **21**, 181–197 (1976).
[71] T. M. Jenkins, W. R. Nelson, and A. Rindi, *Monte Carlo Transport of Electrons and Photons* (Plenum, New York, 1988).
[72] P. Andreo, "Monte Carlo techniques in medical radiation physics," Phys. Med. Biol. **36**, 861–920 (1991).
[73] D. W. O. Rogers, B. A. Faddegon, G. X. Ding, C.-M. Ma, and J. We, "Beam: A Monte Carlo code to simulate radiotherapy treatment units," Med. Phys. **22**, 503–524 (1995).
[74] W. R. Nelson, H. Hirayama, and D. W. O. Rogers (Rep. 265), *The EGS4 code System* (Stanford Linear Accelerator Center, 1985).
[75] R. Nath, E. R. Epp, J. S. Laughlin, W. P. Swanson, and V. P. Bond, "Neutrons from high energy x-ray medical accelerators: An estimate of risk to the radiotherapy patient," Med. Phys. **11**, 231–241 (1984).
[76] NCRP Report #79, "Neutron contamination from medical electron accelerators" (1984).
[77] N. Adnani, "High energy linac neutrons: Applications to neutron capture therapy and in-situ activation brachytherapy," presented at the WC2000, Chicago, 2000.
[78] M. Essers and B. J. Mijnheer, "In vivo dosimetry during external photon beam radiotherapy: current clinical practice," Int. J. Radiat. Oncol., Biol., Phys. **43**, 245–259 (1999).
[79] R. Alecu, M. Alecu, and T. G. Ochran, "A method to improve the effectiveness of diode in vivo dosimetry," Med. Phys. **25**, 746–749 (1998).
[80] R. Alecu, J. J. Feldmeier, and M. Alecu, "Dose perturbations due to in vivo dosimetry with diodes," Radiother. Oncol. **42**, 289–291 (1997).
[81] R. Alecu, T. Loomis, J. Alecu, and T. Ochran, "Guidelines on the implementation of diode in vivo dosimetry programs for photon and electron beam therapy," Med. Dosim **24**, 5–12 (1999).
[82] J. Van Dam and G. Marinello, "Methods for in vivo dosimetry in external

radiotherapy,'' ESTRO Booklet No 1, European Society for Therapeutic Radiology, Brussels, 1994.
[83] ''Practical guidelines for the implementation of in vivo dosimetry with diodes in external radiotherapy with photon beams (entrance dose),'' ESTRO Booklet No 5, European Society for Therapeutic Radiology, Brussels, 2001.
[84] J. Van Dam, C. Vaerman, N. Blanckaert, G. Leunens, A. Dutreix, and E. van der Schueren, ''Are port films reliable for in vivo exit dose measurements?'' Radiother. Oncol. **25**, 67–72 (1992).
[85] X. G. Ying, L. Y. Geer, and J. W. Wong, ''Portal dose images. II: Patient dose estimation,'' Int. J. Radiat. Oncol., Biol., Phys. **18**, 1465–1475 (1990).
[86] R. McNutt, T. R. Mackie, P. Reckwerdt, and B. R. Paliwal, ''Modelling dose distributions from portal images using the convolution/superposition method,'' Med. Phys. **23**, 1381–1392 (1996).
[87] R. Boellaard, M. van Herk, H. Uiterwaal, and B. Mijnheer, ''First clinical tests using a liquid-filled electronic portal imaging device and a convolution model for the verification of the midplane dose,'' Radiother. Oncol. **47**, 303–312 (1998).
[88] J. H. Kung, C. Reft, W. Jackson, and I. Abdalla, ''Intensity Modulated Radiotherapy for a prostate patient with a metal prothesis,'' Med. Dosim. **26**, 305–308 (2001).
[89] T. Bortfeld, W. Schlegel, and B. Rhein, ''Decomposition of pencil beam kernels for fast dose calculations in three-dimensional treatment planning,'' Med. Phys. **20**(2, Pt. 1), 311–318 (1993).
[90] M. R. Sontag and J. R. Cunningham, ''The equivalent tissue-air ratio method for making absorbed dose calculations in a heterogeneous medium,'' Radiology **129**, 787–794 (1978).
[91] C. X. Yu and J. W. Wong, ''Implementation of the ETAR method for 3D inhomogeneity correction using FFT,'' Med. Phys. **20**, 627–632 (1993).